An overview of η and η′ decays at BESIII *

Shuang-shi Fang(房双世)[1,2,3;1)] Andrzej Kupsc[4;2)] Dai-hui Wei(魏代会)[3;3)]

[1] Institute of High Energy Physics, Chinese Academy of Science, Beijing 100049, China
[2] University of Chinese Academy of Sciences, Beijing 100049, China
[3] Guangxi Normal University, Guilin 541004, China
[4] Uppsala University, Box 516, SE-75120 Uppsala, Sweden

Abstract: The world's largest sample of J/ψ events, 1.31 billion events accumulated at the BESIII detector, provides a unique opportunity to investigate η and η′ physics via two-body J/ψ radiative or hadronic decays. For many η′ decay channels the low background data samples are up to three orders of magnitude larger than collected in any previous experiment. Here we review the most significant results on η and η′ obtained at BESIII so far. The analyses range from detailed studies of common decay dynamics, observations of new radiative and Dalitz decays, and searches for rare/forbidden decays with sensitivity up to $\mathcal{B}\sim10^{-5}$. Finally, prospects of forthcoming runs at the J/ψ peak for η and η′ physics are discussed.

Keywords: η/η′ decays, the BESIII detector, J/ψ decays

PACS: 13.20.-v, 14.40.Be **DOI:** 10.1088/1674-1137/42/4/042002

1 Introduction

More than half a century after the discoveries of the η [1] and η′ [2, 3], these mesons still attract the attention of both theory and experiment. As the neutral members of the ground state pseudoscalar nonet, they play an important role in understanding low energy quantum chromodynamics (QCD). The main properties of the η and η′ mesons are firmly established and their main decay modes are fairly well known. Decays of the η/η′ probe a wide variety of physics issues, *e.g.* $\pi^0-\eta$ mixing, light quark masses and pion-pion scattering. In particular the η′ meson, much heavier than the Goldstone bosons of broken chiral symmetry, plays a special role as the predominant singlet state arising from the strong axial $U(1)$ anomaly. In addition, the decays of both mesons are used to search for processes beyond any considered extension of the Standard Model (SM) and to test fundamental discrete symmetries.

The main decays of the η/η′ meson are hadronic and radiative processes. Alternatively, one can divide the decays into the two following classes. The first class consists of hadronic decays into three pseudoscalar mesons, such as $\eta' \to \eta\pi\pi$. Those processes are already included in the lowest order, $\mathcal{O}(p^2)$, of chiral perturbation theory (ChPT) [4]. The second class includes anomalous processes involving an odd number of pseudoscalar mesons, such as $\eta' \to \rho^0\gamma$ and $\eta' \to \pi^+\pi^-\pi^+\pi^-$. They are driven by the Weiss-Zumino-Witten (WZW) term [5, 6] which enters at $\mathcal{O}(p^4)$ order [7]. The dynamics of η decays remains a subject of extensive studies aiming at precision tests of ChPT in the $SU_L(3)\times SU_R(3)$ sector (*i.e.* involving an s quark). Model-dependent approaches for describing low energy meson interactions, such as vector meson dominance (VMD) [8, 9], and the large number of colors, N_C, extensions of ChPT [10], together with dispersive methods, could be extensively tested in η′ decays.

The BESIII detector [16], operating at the Beijing Electron Positron Collider (BEPCII), is a general purpose facility designed for τ-charm physics studies in e^+e^- annihilation with high precision. Since its commissioning in 2008, a series of important results has been achieved, including charmonium decays, light hadron spectroscopy and charm meson decay, with the world's largest data samples in the τ-charm region. Due to the high production rate of light mesons in charmonium, *e.g.*, J/ψ, decays, the BESIII experiment also offers a unique possibility to investigate the light meson decays. The radiative decays $J/\psi \to \eta\gamma$ and $J/\psi \to \eta'\gamma$ provide clean and efficient sources of η/η′ mesons for the decay studies. The accompanying radiative photon, with energy of

Received 15 December 2017, Published online 15 March 2018
∗ Supported by National Natural Science Foundation of China (NSFC) (11565006, 11675184, 11735014)
1) E-mail: fangss@ihep.ac.cn
2) E-mail: Andrzej.Kupsc@physics.uu.se
3) E-mail: weidh@gxnu.edu.cn
©2018 Chinese Physical Society and the Institute of High Energy Physics of the Chinese Academy of Sciences and the Institute of Modern Physics of the Chinese Academy of Sciences and IOP Publishing Ltd

1.5 GeV/c^2 and 1.4 GeV/c^2 respectively, is well separated from the decay products. An alternative source of the η (η') is the hadronic two-body process of $J/\psi\to\phi\eta$ ($J/\psi\to\phi\eta'$) where ϕ is identified via $\phi\to K^+K^-$ decay and could be used to tag $\eta(\eta')$ decays where not all the decay products are reconstructed.

With two runs in 2009 and in 2012, a total data sample of 1.31×10^9 J/ψ events [18, 19] was collected at the BESIII detector. The available η and η' events from radiative decays of $J/\psi\to\gamma\eta$, $\gamma\eta'$, and hadronic decays of $J/\psi\to\phi\eta$, $\phi\eta'$, are summarized in Table 1.

Table 1. The available η/η' decays calculated with the 1.31×10^9 J/ψ events at BESIII.

decay mode	$\mathcal{B}$ ($\times10^{-4}$) [17]	η/η' events
$J/\psi\to\gamma\eta'$	51.5±1.6	6.7×10^6
$J/\psi\to\gamma\eta$	11.04±0.34	1.4×10^6
$J/\psi\to\phi\eta'$	7.5±0.8	9.8×10^5
$J/\psi\to\phi\eta$	4.5±0.5	5.9×10^5

The review presents recent progress on η/η' decays at the BESIII experiment. Unless specifically mentioned, the analyses are based on the full data sample of 1.31×10^9 J/ψ events. However, some earlier analyses use data from the 2009 run only with 225.3×10^6 J/ψ events. A summary of some branching fractions measured by BESIII and the collected data samples using the full data set is presented in Table 2. For the common three body η and η' processes, results on the decay distributions are reported. In addition, the upper limits at 90% confidence level (C.L.) for rare and forbidden decay modes are presented. Finally, the prospects for the analyses based on the 10^{10} J/ψ events to be collected at BESIII in the near future are discussed.

2 η/η' hadronic decays

2.1 $\eta\to\pi^+\pi^-\pi^0$ and $\eta\to\pi^0\pi^0\pi^0$ [20]

Decays of the η meson into 3π violate isospin symmetry and were first considered to be electromagnetic transitions. However, it turns out that the electromagnetic contribution is strongly suppressed [21–24]. Therefore the decays provide a unique opportunity for a precision determination of the m_u/m_d quark mass ratio in a strong process [25]. The challenge for the theory is to provide a model independent description of the process based on ChPT, supplemented by general analytic properties of the amplitudes (dispersive methods). This approach looks promising to finally resolve the long standing discrepancy between the lowest order ChPT prediction for the decay width of $\eta\to\pi^+\pi^-\pi^0$ of 66 eV [26] and the experimental value of 300±11 eV [17]. This would conclude several years of effort invested by several theory groups in understanding the problem, see *e.g.* [27–35]. However, now there is a need for high statistics Dalitz plot distributions of $\eta\to\pi^+\pi^-\pi^0$ to test and/or constrain the theoretical predictions.

With the radiative decay $J/\psi\to\gamma\eta$, a clean sample of 8×10^4 $\eta\to\pi^+\pi^-\pi^0$ candidate events was selected at BESIII. Figure 1(a) shows the $\pi^+\pi^-\pi^0$ invariant mass, with the pronounced η peak and ∼0.1% background.

The two Dalitz plot variables are defined as $X=\sqrt{3}(T_{\pi^+}-T_{\pi^-})/Q$ and $Y=3T_{\pi^0}/Q-1$, where T_π denotes the kinetic energy of a pion in the η rest frame and $Q=m_\eta-m_{\pi^+}-m_{\pi^-}-m_{\pi^0}$ is the excess energy of the reaction. The distributions of X and Y are shown in Figs. 1 (b) and (c). Using the same parameterization as in Ref. [36], the decay amplitude squared is expressed as

$$|A(X,Y)|^2\propto1+aY+bY^2+cX+dX^2 +eXY+fY^3+\ldots, \quad (1)$$

where the coefficients a,b,c,... are the Dalitz plot parameters. Terms with odd powers of X (c and e parameters) are included only to test charge conjugation (C) conservation. An unbinned maximum likelihood fit to data gives the Dalitz plot parameters shown in Table 3 where they are compared to the results from previous measurements and theoretical calculations. The effect of including the c and e parameters was tested in an alternative fit. The a, b, d and f parameters are almost unchanged, while the parameters c and e are consistent with zero within one standard deviation.

For $\eta\to\pi^0\pi^0\pi^0$, the amplitude squared is nearly constant and the deviation can be parameterized in the lowest order using just one variable $Z=\frac{2}{3}\sum_{i=1}^{3}(3T_i/Q-1)^2$, where $Q=m_\eta-3m_{\pi^0}$ and T_i denotes the kinetic energy of each π^0 in the η rest frame. The Dalitz plot density distribution could be parameterized using a linear term,

$$|A(Z)|^2\propto1+2\alpha Z+\ldots, \quad (2)$$

where α is the slope parameter.

The $\pi^0\pi^0\pi^0$ mass spectrum is shown in Fig. 2(a), with the η peak and the background estimated to be less than 1%. The distribution of the variable Z is displayed in Fig. 2(b). Due to the kinematic boundaries and the cusp at the $\pi^0\pi^0\to\pi^+\pi^-$ threshold [31, 43], only the interval of $0<Z<0.7$ is used to extract the slope parameter α from the data. In analogy with the $\eta\to\pi^+\pi^-\pi^0$ measurement an unbinned maximum likelihood fit, as displayed in the inset of Fig. 2(b), yields the Dalitz plot slope parameter $\alpha=-0.055\pm0.014\pm0.004$, which is compatible with the recent results from other experiments.

2.2 $\eta'\to\pi^+\pi^-\eta$ [50] and $\eta'\to\pi^{+(0)}\pi^{-(0)}\eta$ [51]

The combined branching fraction of the two main hadronic decays of η' – $\eta'\to\pi^+\pi^-\eta$ and $\eta'\to\pi^0\pi^0\eta$ – is nearly 2/3. The ratio $\mathcal{B}(\eta'\to\pi^+\pi^-\eta)/\mathcal{B}(\eta'\to\pi^0\pi^0\eta)$

Table 2. Some of the BESIII results on η' branching fractions, $\mathcal{B}$, based on the sample of 1.31×10^9 J/ψ events. Extracted yields are given with statistical errors, detection efficiency and branching fractions for the studied η' decay modes, where the first error is statistical, the second systematic, and the third from model dependence. The last column gives the status before the BESIII experiment.

decay mode	Yield	ε (%)	$\mathcal{B}$ ($\times10^{-4}$)	Ref.	comment
$\eta'\to\pi^+\pi^-\pi^0$	6067 ± 91	25.3	35.91 ±0.54±1.74	[11]	previously 20 events
$(\pi^+\pi^-\pi^0)_S$	6580 ± 130	26.2	37.63±0.77±2.22±4.48	[11]	first measurement
$\rho^\pm\pi^\mp$	1231 ± 98	24.8	7.44±0.60±1.26±1.84	[11]	first measurement
$\eta'\to\pi^0\pi^0\pi^0$	2015 ± 47	8.8	35.22±0.82±2.60	[11]	previously 235 events
$\eta'\to e^+e^-\gamma$	864± 36	24.5	4.69±0.20±0.23	[12]	first measurement
$\eta'\to e^+e^-\omega$	66±11	5.45	1.97± 0.34±0.17	[13]	first measurement
$\eta'\to\gamma\omega$	33187 ± 351	21.9	255.00±3.00±16.00	[13]	
$\eta'\to\gamma\gamma\pi^0$	655 ± 68	15.9	6.16±0.64±0.67	[14]	first measurement
$\eta'\to\pi^+\pi^-\pi^+\pi^-$	199 ±16	34.5	0.853 ±0.069±0.069	[15]	first measurement
$\eta'\to\pi^+\pi^-\pi^0\pi^0$	84 ±16	7.0	1.82±0.35±0.18	[15]	first measurement

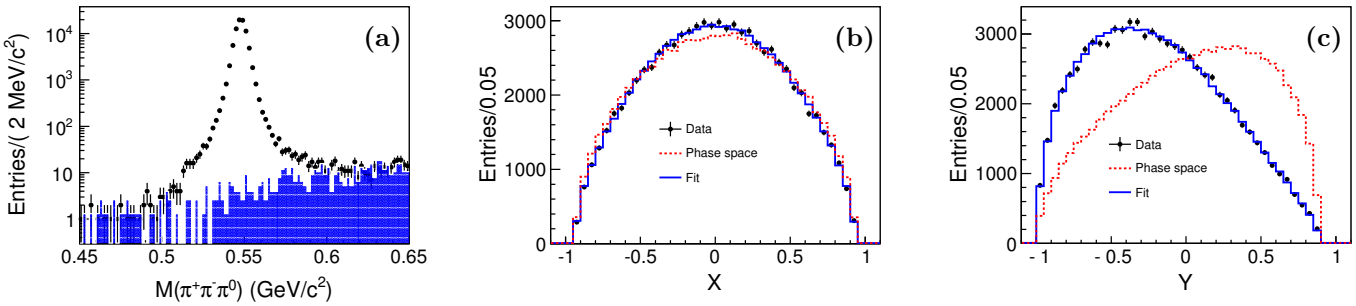

Fig. 1. (color online) (a) Distribution of $\pi^+\pi^-\pi^0$ invariant mass. Projections of the Dalitz plot as a function of (b) X and (c) Y for $\eta\to\pi^+\pi^-\pi^0$ obtained from data (dots with error bars), the fit projections (solid line) and phase space distributed MC events (dashed line). Reprinted figures with permission from M. Ablikim et al, Phys. Rev. D 92, 012014, 2015 (DOI: https://doi.org/10.1103/PhysRevD.92.012014) (Ref. [20]). Copyright 2015 by the American Physical Society.

Table 3. Theoretical and experimental values for the $\eta\to\pi^+\pi^-\pi^0$ Dalitz plot parameters.

theory/Exp.	a	b	d	f
ChPT NLO[27]	−1.33	0.42	0.08	0
ChPT NNLO[30]	−1.271±0.075	0.394±0.102	0.055±0.057	0.025±0.160
Dispersive Theory[28]	−1.16	0.26	0.10	0
Absolute Dispersive[37]	−1.21	0.33	0.04	0
UA[38]	−1.049±0.025	0.178±0.019	0.079±0.028	0.064±0.012
NREFT[31]	−1.218±0.013	0.314±0.023	0.051±0.003	0.084±0.019
Layter[39]	−1.08±0.014	0.03±0.03	0.05±0.03	–
CBarrel[40]	−1.22±0.07	0.22±0.11	0.06($fixed$)	–
KLOE08[36]	$-1.09^{+0.013}_{-0.024}$	0.124±0.016	$0.057^{+0.016}_{-0.022}$	0.14±0.03
WASA-at-COSY[41]	−1.144±0.018	0.219±0.019±0.047	0.086±0.018±0.015	0.115±0.037
BESIII[20]	−1.128±0.015±0.008	0.153±0.017±0.004	0.085±0.016±0.009	0.173±0.028±0.021
KLOE16[42]	−1.104±0.003±0.002	$0.142\pm0.003^{+0.005}_{-0.004}$	$0.073\pm0.003^{+0.004}_{-0.003}$	$0.154\pm0.006^{+0.004}_{-0.005}$

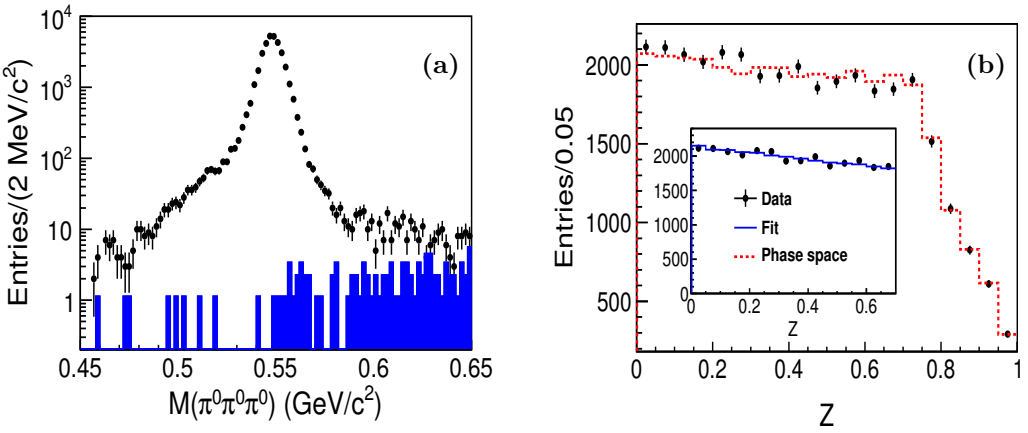

Fig. 2. (color online) (a) Distribution of $M(\pi^0\pi^0\pi^0)$ in the η mass region. (b) Distribution of the variable Z for $\eta\to\pi^0\pi^0\pi^0$. Dots with error bars are for data, histograms for background contributions, dashed histograms for phase space distributed MC events and the solid lines in the inset are the results of the fit. Reprinted figure with permission from M. Ablikim et al, Phys. Rev. D 92, 012014, 2015 (DOI: https://doi.org/10.1103/PhysRevD.92.012014) (Ref. [20]). Copyright 2015 by the American Physical Society.

should be exactly two in the isospin limit. The decays involve both η and pions in the final state and therefore allows extraction of information about $\pi\eta$ interactions. However, the excess energy of the processes is relatively small: 130 MeV and 140 MeV for $\pi^+\pi^-\eta$ and $\pi^0\pi^0\eta$ respectively. This means precision high statistics experimental studies of the Dalitz plots together with an appropriate theory framework for extraction of the $\pi\eta$ phase shifts are needed.

Table 4. Theoretical and experimental values for $\eta\to\pi^0\pi^0\pi^0$ Dalitz plot slope parameter α.

theory/Exp.	α
ChPT/NLO[27]	0.015
dispersive[28]	(-0.014)-(-0.007)
UA[38]	-0.031 ± 0.003
ChPT/NNLO[30]	0.013 ± 0.032
KLOE[44]	$-0.0301\pm0.0035^{+0.0022}_{-0.0035}$
WASA-at-COSY[45]	$-0.027\pm0.008\pm0.005$
CBall[46]	$-0.0322\pm0.0012\pm0.0022$
SND[47]	$-0.010\pm0.021\pm0.010$
CBarrel[48]	$-0.052\pm0.017\pm0.010$
GAM2[49]	-0.022 ± 0.023
BESIII[20]	$-0.055\pm0.014\pm0.004$

The two Dalitz plot variables, X and Y, are usually defined as $X=\frac{\sqrt{3}}{Q}(T_{\pi^+}-T_{\pi^-})$ and $Y=\frac{m_\eta+2m_\pi}{m_\pi}\frac{T_\eta}{Q}-1$, where $T_{\pi,\eta}$ denote the kinetic energies of the mesons in the η' rest frame and $Q=T_\eta+T_{\pi^+}+T_{\pi^-}=m_{\eta'}-m_\eta-2m_\pi$.

Two different parametrizations of the Dalitz plot distribution are used. The historically first one assumes a linear amplitude in the Y variable:

$$|A(X,Y)|^2\propto|1+\alpha Y|^2+cX+dX^2, \quad (3)$$

and the other representation is just a general polynomial expansion:

$$|A(X,Y)|^2\propto1+aY+bY^2+cX+dX^2, \quad (4)$$

where α is complex and a, b, c, d are real parameters. These two representations are equivalent in the case of $b>a^2/4$.

Initial BESIII $\eta'\to\pi^+\pi^-\eta$ Dalitz plot analysis [50] was based on 2009 data and the above two representations were used. The extracted parameters are generally consistent with the previous measurements and theoretical predictions. The negative value of the b parameter indicates, with an uncertainty of 30%, that the two representations may not be equivalent. The most recent BESIII analysis [51] uses nearly background-free samples of 3.5×10^5 $\eta'\to\eta\pi^+\pi^-$ events and 5.6×10^4 $\eta'\to\eta\pi^0\pi^0$ events from 1.31×10^9 J/ψ. The goal was determination of the Dalitz plot parameters for the two decay modes and a search for the cusp at the $\pi^0\pi^0\to\pi^+\pi^-$ threshold in $\eta'\to\eta\pi^0\pi^0$. The Dalitz plots for data in terms of variables X and Y for the two decays are shown in Fig. 3(a) and Fig. 3(b), respectively. The fit results for the two representations are compared to the X and Y projections for data in Fig. 4 and Fig. 5, and the corresponding fitted parameters are summarized in Table 5.

For the $\eta'\to\eta\pi^+\pi^-$ decay, the results, superseding the previous BESIII measurement [50], are not consistent with the measurement from VES and the theoretical predictions within the framework of $U(3)$ chiral effective field theory in combination with a relativistic coupled-channels method (chiral unitary approach – ChUA) [38]. In particular, for the cofficient a the discrepancies are about four standard deviations. On the other hand, the

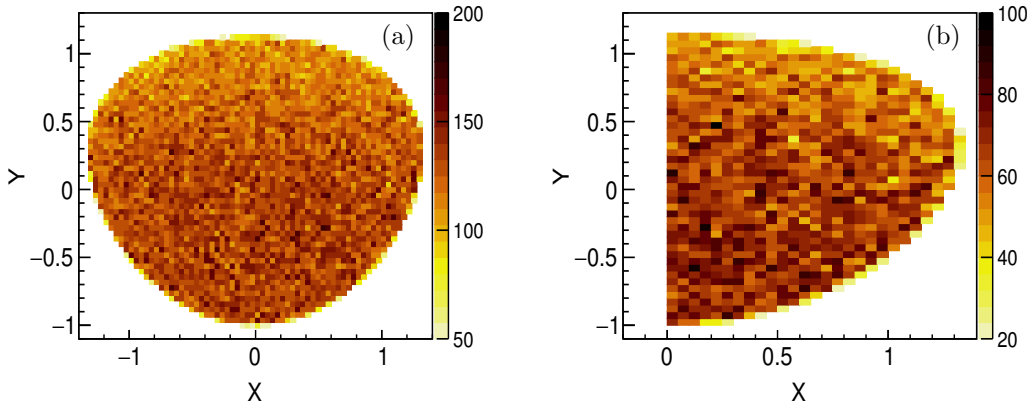

Fig. 3. (color online) The experimental Dalitz plots for the decays $\eta'\to\pi^+\pi^-\eta$ (a) and $\eta'\to\pi^0\pi^0\eta$ (b) in terms of the variables X and Y.

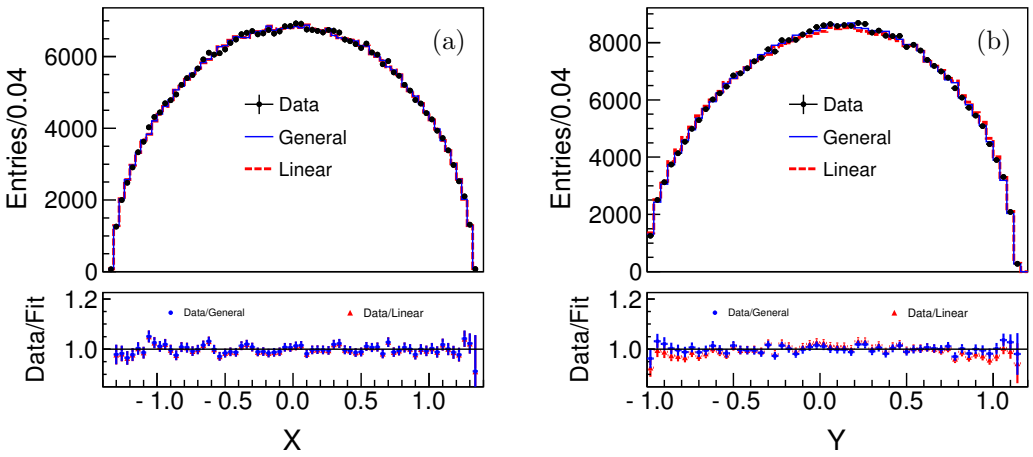

Fig. 4. (color online) The distributions of variables X (a) and Y (b), where the dashed histograms are from MC of $\eta'\to\pi^+\pi^-\eta$ events generated with phase space. The solid histograms are the fit results described in the text.

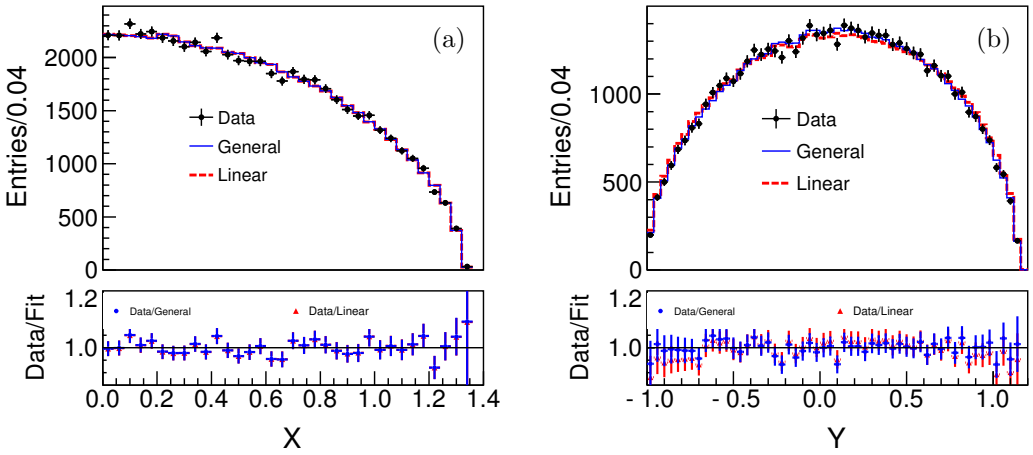

Fig. 5. (color online) The distributions of variables X (a) and Y (b), where the dashed histograms are from MC of $\eta'\to\pi^0\pi^0\eta$ events generated with phase space. The solid histograms are the fit results described in the text.

Table 5. Experimental and theoretical values of the Dalitz plot parameters for $\eta'\to\eta\pi^+\pi^-$ and $\eta'\to\eta\pi^0\pi^0$. The values for parameter c and $\Im(\alpha)$ are given only for comparison with previous experiments.

Para.	$\eta'\to\eta\pi^+\pi^-$				$\eta'\to\eta\pi^0\pi^0$		
	ChUA [38]	Large N_C [52]	VES [53]	BESIII [51]	ChUA [38]	GAMS-4π [54]	BESIII [51]
a	-0.116 ± 0.011	-0.098 ± 0.048	-0.127 ± 0.018	$-0.056\pm0.004\pm0.003$	-0.127 ± 0.009	-0.067 ± 0.016	$-0.087\pm0.009\pm0.006$
b	-0.042 ± 0.034	-0.050 ± 0.001	-0.106 ± 0.032	$-0.049\pm0.006\pm0.006$	-0.049 ± 0.036	-0.064 ± 0.029	$-0.073\pm0.014\pm0.005$
c	...	...	$+0.015\pm0.018$	$(2.7\pm2.4\pm1.8)\times10^{-3}$	...	...	...
d	$+0.010\pm0.019$	-0.092 ± 0.008	-0.082 ± 0.019	$-0.063\pm0.004\pm0.004$	$+0.011\pm0.021$	-0.067 ± 0.020	$-0.074\pm0.009\pm0.004$
$\Re(\alpha)$	...	...	-0.072 ± 0.014	$-0.034\pm0.002\pm0.002$	...	-0.042 ± 0.008	$-0.054\pm0.004\pm0.001$
$\Im(\alpha)$	...	...	0.000 ± 0.100	$0.000\pm0.019\pm0.001$	...	0.000 ± 0.070	$0.000\pm0.038\pm0.002$
c	...	...	$+0.020\pm0.019$	$(2.7\pm2.4\pm1.5)\times10^{-3}$	...	...	...
d	...	...	-0.066 ± 0.034	$-0.053\pm0.004\pm0.004$	...	-0.054 ± 0.019	$-0.061\pm0.009\pm0.006$

large-N_C ChPT prediction at next-to-next-to-leading order [52] is consistent with the measured a value due to the large theoretical uncertainty. For the cofficient c violating charge conjugation, the fitted values are consistent with zero within one standard deviation for both representations.

In the case of $\eta'\to\eta\pi^0\pi^0$, the results are in general consistent with the previous measurements and theoretical predictions within the uncertainties from both sides. The latest results [55] reported by the A2 experiment are also in agreement with those obtained from BESIII. We notice a discrepancy of 2.6 standard deviations for parameter a between $\eta'\to\eta\pi^+\pi^-$ and $\eta'\to\eta\pi^0\pi^0$ modes. The present results are not precise enough to firmly establish isospin violation and additional effects, *e.g.*, radiative corrections [56] and the π^+/π^0 mass difference should be considered in future experimental and theoretical studies.

It was also found that the linear representation could not describe the data. The discrepancies between the data and the fit are evident in the Y projection for the both decay modes, which is yet another indication that the linear and general representations are not equivalent. In addition, a search for the cusp in $\eta'\to\eta\pi^0\pi^0$, performed by inspecting the $\pi^0\pi^0$ mass spectrum close to the $\pi^+\pi^-$ mass threshold, reveals no statistically significant effect. Most recent theoretical dispersive analysis of the cusp in the $\eta'\to\eta\pi^0\pi^0$ [57] uses Dalitz plot parameters from VES and 2009 BESIII[50] $\eta'\to\eta\pi^+\pi^-$ data. However, the amplitudes from Ref. [57] should be preferably fitted directly to the Dalitz plot data for the two decay modes.

2.3 $\eta'\to\pi^0\pi^0\pi^0$ [20]

The isospin violating decay of $\eta'\to\pi^0\pi^0\pi^0$ was first observed in $\pi^-\mathrm{p}\to\eta\mathrm{n}$ [58]. In a later experiment the Dalitz plot slope parameter was extracted to be $\alpha=-0.1\pm0.3$ with limited statistics of around 60 events [59], and in 2008 the GAMS-4π analysis updated this to $\alpha=-0.59\pm0.18$ using 235 ± 45 events [54]. Using the 2009 J/ψ data sample, BESIII has reported the branching fraction of the decay, which is about two times larger than that of Ref. [54, 58, 59] (average $\mathcal{B}=(1.77\pm0.23)\times10^{-3}$ for the three experiments). However, in this first BESIII analysis the Dalitz plot slope parameter was not reported [60].

With the full J/ψ data set a determination of the Dalitz plot slope was possible [20]. The η' signal is clearly observed in the $\pi^0\pi^0\pi^0$ mass spectrum, Fig. 6(a), where the hatched and shaded histograms show the background contributions from the inclusive J/ψ decays and $\eta'\to\pi^0\pi^0\eta$, respectively. As shown in Fig. 6(b), a maximum-likelihood fit to the events with Z in the region of $0.2<Z<0.6$ gives the Dalitz plot slope parameter: $\alpha=-0.640\pm0.046\pm0.047$, much more precise than previous measurements, as summarized in Table 6. The value deviates significantly from zero, which implies that final state interactions play an important role. Up to now, there have only been a few theory predictions to compare the parameter value. One exception is the ChUA calculations of Ref. [38]. The predicted value of the α coefficient is in the -2.7 to 0.1 range, consistent with the BESIII measurement.

Table 6. Theoretical and experimental values for the $\eta'\to\pi^0\pi^0\pi^0$ Dalitz plot slope parameter α.

theory/exp.	α
ChUA[38]	$-2.7\sim0.1$
GAMS[54]	-0.59 ± 0.18
GAM2[59]	-0.1 ± 0.3
BESIII[20]	$-0.640\pm0.046\pm0.047$

2.4 Amplitude analysis of $\eta'\to\pi^{+(0)}\pi^{-(0)}\pi^0$ [11]

At first, the low intensity process $\eta'\to\pi^+\pi^-\pi^0$ may be considered to come from π^0–η mixing in the dominating decay $\eta'\to\pi^+\pi^-\eta$ [61]. This would offer a possibility to determine precisely the $u-d$ quark mass difference from the branching fraction ratio of the two processes. However, a recent analysis shows that even at tree level other terms are needed [62]. In addition, the decay amplitudes are strongly affected by the intermediate resonances. Therefore the mixing of π^0–η and the u-d quark mass difference cannot be extracted in a simple way.

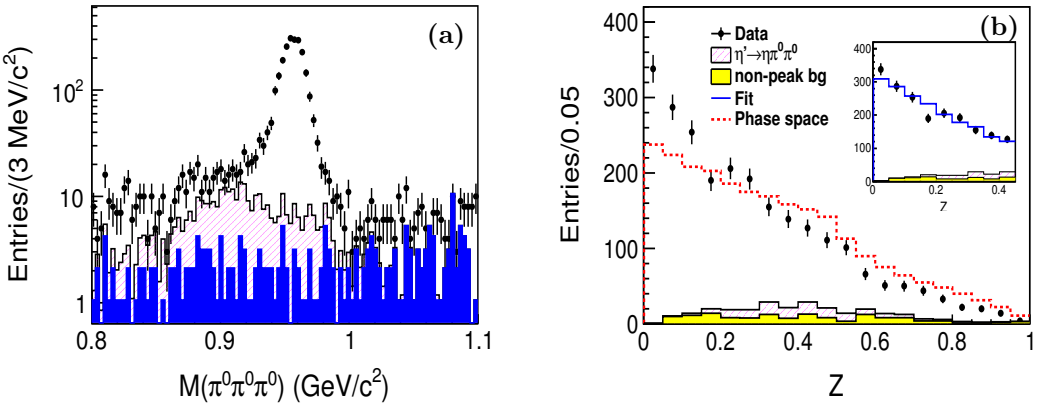

Fig. 6. (color online) (a) Distribution of $M(\pi^0\pi^0\pi^0)$ in the η' mass region. (b) Distribution of the variable Z for $\eta'\to\pi^0\pi^0\pi^0$. Dots with error bars are for data, histograms for background contributions, dashed histograms for phase space distributed MC events and the solid lines in the inset are the results of the fit. Reprinted figure with permission from M. Ablikim et al, Phys. Rev. D 92, 012014, 2015 (DOI: https://doi.org/10.1103/PhysRevD.92.012014) (Ref. [20]). Copyright 2015 by the American Physical Society.

The decay $\eta'\to\pi^+\pi^-\pi^0$ was first observed by the CLEO experiment [63] in 2008. BESIII has reported the branching fraction measurement using 2009 J/ψ data set [60] but the amplitude analysis was only possible with the full data set. In particular it was expected that the contribution of $\eta'\to\rho^\pm\pi^\mp$ could be identified. This expectation is supported by the experimental distributions shown in the Dalitz plot of $M^2(\pi^+\pi^-)$ versus $M^2(\pi^-\pi^0)$ in Fig. 7, where the two clusters corresponding to the contribution $\eta'\to\rho^\pm\pi^\mp$ are seen.

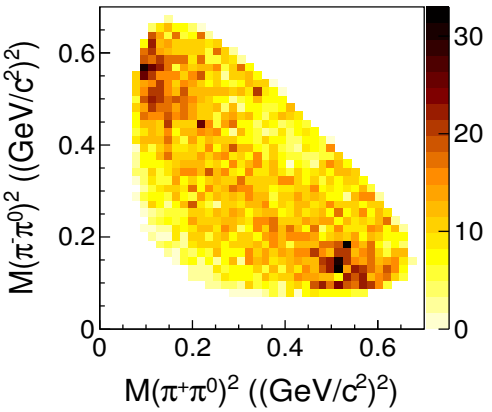

Fig. 7. (color online) Dalitz plot of $M^2(\pi^+\pi^0)$ versus $M^2(\pi^-\pi^0)$ for $\eta'\to\pi^+\pi^-\pi^0$. Reprinted figure with permission from M. Ablikim et al, Phys. Rev. Lett. 118, 012001, 2017 (DOI: https://doi.org/10.1103/PhysRevLett.118.012001) (Ref. [11]). Copyright 2017 by the American Physical Society.

The common amplitude analysis of the decays $\eta'\to\pi^+\pi^-\pi^0$ and $\eta'\to\pi^0\pi^0\pi^0$ is performed using the isobar model. The fit results illustrated by the invariant mass spectra of $\pi^+\pi^-$, $\pi^+\pi^0$ and $\pi^-\pi^0$ (Fig. 8) show a significant P-wave contribution from $\eta'\to\rho^\pm\pi^\mp$ in $\eta'\to\pi^+\pi^-\pi^0$. The branching fraction $\mathcal{B}(\eta'\to\rho^\pm\pi^\mp)$ is determined to be $(7.44\pm0.60\pm1.26\pm1.84_{\rm model})\times10^{-4}$. In addition to the non-resonant S-wave, the resonant π-π S-wave with a pole at $(512\pm15)-i(188\pm12)$ MeV, interpreted as the broad σ meson, plays an essential role in the $\eta'\to\pi\pi\pi$ decays. Due to the large interference between non-resonant and resonant S-waves, only the sum is used to describe the S-wave contribution, and the branching fraction is determined to be $\mathcal{B}(\eta'\to\pi^+\pi^-\pi^0)_S=(37.63\pm0.77\pm2.22\pm4.48_{\rm model})\times10^{-4}$.

For $\eta'\to\pi^0\pi^0\pi^0$, the P-wave contribution in two-body rescattering is forbidden by Bose symmetry. The Dalitz plot for $\eta'\to\pi^0\pi^0\pi^0$ is shown in Fig. 9(a) and the amplitude fit is displayed in Fig. 9(b). The corresponding branching fraction is measured to be $\mathcal{B}(\eta'\to\pi^0\pi^0\pi^0)=(35.22\pm0.82\pm2.60)\times10^{-4}$.

The branching fractions of $\eta'\to\pi^+\pi^-\pi^0$ and $\eta'\to\pi^0\pi^0\pi^0$ are in good agreement with and supersede the previous BESIII measurements [60]. The value for $\mathcal{B}(\eta'\to\pi^0\pi^0\pi^0)$ is two times larger than the GAMS measurement of $(16\pm3.2)\times10^{-4}$ [59]. The significant resonant S-wave contribution also provides a reasonable explanation for the negative slope parameter of the $\eta'\to\pi^0\pi^0\pi^0$ Dalitz plot [20]. The ratio between the S-wave components of the two decay modes, $\mathcal{B}(\eta'\to\pi^0\pi^0\pi^0)/\mathcal{B}(\eta'\to\pi^+\pi^-\pi^0)_S$, is determined to be $0.94\pm0.029\pm0.13$, where the common systematic cancels. With the branching fractions of $\eta'\to\pi\pi\eta$ taken from the Particle Data Group (PDG) [17], $r_\pm=\mathcal{B}(\eta'\to\pi^+\pi^-\pi^0)/\mathcal{B}(\eta'\to\pi^+\pi^-\eta)$ and $r_0=\mathcal{B}(\eta'\to\pi^0\pi^0\pi^0)/\mathcal{B}(\eta'\to\pi^0\pi^0\eta)$ are calculated to be $(8.8\pm1.2)\times10^{-3}$ and $(16.9\pm1.4)\times10^{-3}$, respectively.

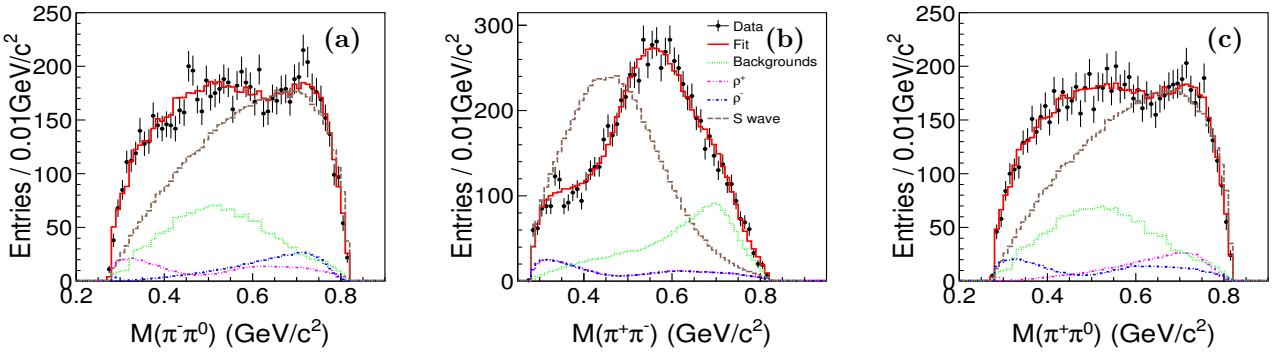

Fig. 8. (color online) Comparison of the invariant mass distributions of (a) $\pi^-\pi^0$, (b) $\pi^+\pi^-$, (c) $\pi^+\pi^0$ (dots with error bars) and the fit projections (solid histograms). The dotted, dashed, dash-dotted, and dash-dot-dotted histograms show the contributions from background, S wave, ρ^-, and ρ^+, respectively. Reprinted figure with permission from M. Ablikim et al, Phys. Rev. Lett. 118, 012001, 2017 (DOI: https://doi.org/10.1103/PhysRevLett.118.012001) (Ref. [11]). Copyright 2017 by the American Physical Society.

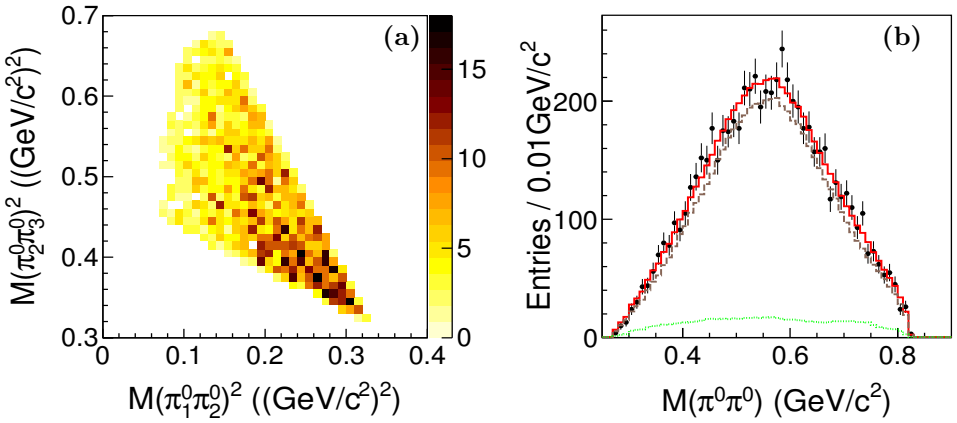

Fig. 9. (color online) (a) Dalitz plot for $\eta'\to\pi^0\pi^0\pi^0$. (b) Comparison of $\pi^0\pi^0$ mass spectrum between data (dots with error bars) and the fit projections (solid histograms). Reprinted figure with permission from M. Ablikim et al, Phys. Rev. Lett. 118, 012001, 2017 (DOI: https://doi.org/10.1103/PhysRevLett.118.012001) (Ref. [11]). Copyright 2017 by the American Physical Society.

2.5 $\eta'\to\pi^+\pi^-\pi^+\pi^-,\pi^+\pi^-\pi^0\pi^0$ [15]

In ChPT, anomalous hadronic decays $\eta'\to\pi^+\pi^-\pi^{+(0)}\pi^{-(0)}$ are related to the WZW pentagon contribution. In the VMD model, $\rho^0\rho^0$ or $\rho^+\rho^-$ intermediate states should provide a dominant contribution. Using a combination of ChPT and VMD, the branching fractions were calculated to be $\mathcal{B}(\eta'\to\pi^+\pi^-\pi^+\pi^-)=(1.0\pm0.3)\times10^{-4}$ and $\mathcal{B}(\eta'\to\pi^+\pi^-\pi^0\pi^0)=(2.4\pm0.7)\times10^{-4}$ [64].

The $\pi^+\pi^-\pi^{+(0)}\pi^{-(0)}$ invariant mass distributions for the BESIII analysis are shown in Figs. 10(a) and (b), respectively, where the η' peak is clearly seen. The results of background simulations are indicated by the hatched histograms in Figs. 10(a) and (b). None of the background sources produces a peak in the $\pi^+\pi^-\pi^{+(0)}\pi^{-(0)}$ invariant mass spectrum near the η' mass.

In order to measure the branching fractions, the signal efficiency was estimated using a signal MC sample using two assumptions: flat phase space and the decay amplitudes from Ref. [64]. For $\eta'\to\pi^+\pi^-\pi^+\pi^-$, each of the $M(\pi^+\pi^-)$ combinations was divided into 38 bins in the region of [0.28, 0.66] GeV/c^2. With the procedure described above, the number of the η' events in each bin was obtained by fitting the $\pi^+\pi^-\pi^+\pi^-$ mass spectrum in this bin, and then the background-subtracted $M(\pi^+\pi^-)$ was obtained as shown in Fig. 11 (four entries per event), where the errors are statistical only. The comparison of the experimental $M(\pi^+\pi^-)$ distribution and two models shown in Fig. 11 indicates that the amplitude of Ref. [64] provides a better description of the data than the phase space. Therefore this amplitude is used in the simulation to determine the detection efficiency for $\eta'\to\pi^+\pi^-\pi^{+(0)}\pi^{-(0)}$ decays.

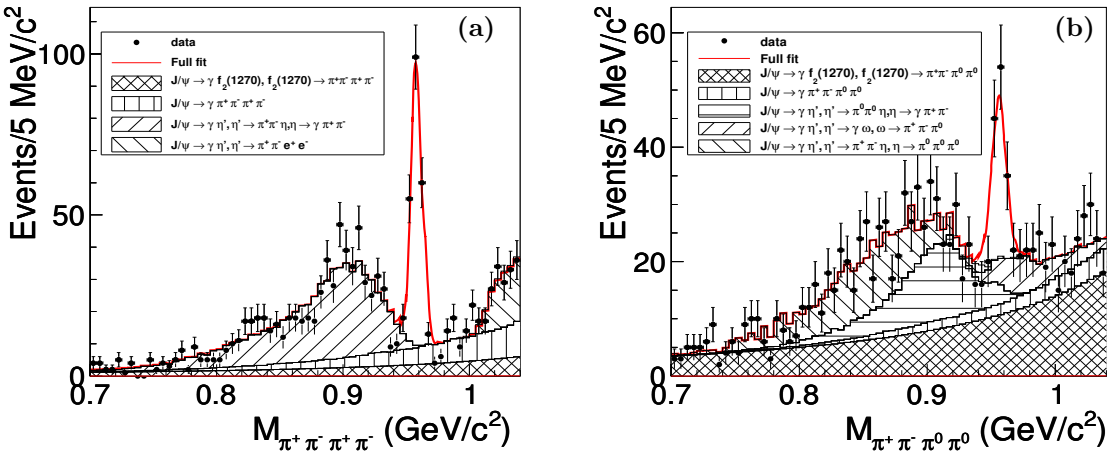

Fig. 10. (color online) Results of the fits to (a) $M(\pi^+\pi^-\pi^+\pi^-)$ and (b) $M(\pi^+\pi^-\pi^0\pi^0)$, where the background contributions are displayed as the hatched histograms. Reprinted figure with permission from M. Ablikim et al, Phys. Rev. Lett. 112, 251801, 2014 (DOI: https://doi.org/10.1103/PhysRevLett.112.251801) (Ref. [15]). Copyright 2014 by the American Physical Society.

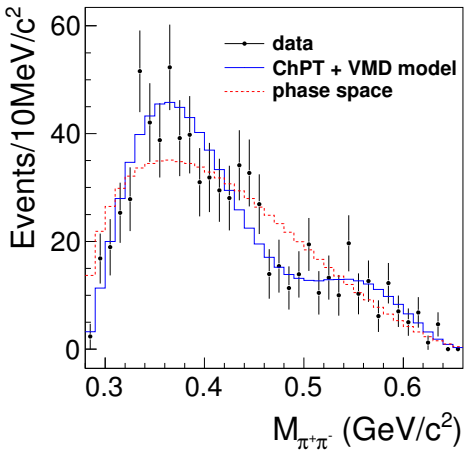

Fig. 11. (color online) The distribution of $M(\pi^+\pi^-)$. Reprinted figure with permission from M. Ablikim et al, Phys. Rev. Lett. 112, 251801, 2014 (DOI: https://doi.org/10.1103/PhysRevLett.112.251801) (Ref. [15]). Copyright 2014 by the American Physical Society.

The signal yields are obtained from extended unbinned maximum likelihood fits to the $\pi^+\pi^-\pi^+\pi^-$ and $\pi^+\pi^-\pi^0\pi^0$ invariant mass distributions and the statistical significances for $\eta'\to\pi^+\pi^-\pi^+\pi^-$ and $\eta'\to\pi^+\pi^-\pi^0\pi^0$ are calculated to be 18σ and 5σ, respectively. The branching fractions of $\eta'\to\pi^+\pi^-\pi^{+(0)}\pi^{-(0)}$ are determined to be $\mathcal{B}(\eta'\to\pi^+\pi^-\pi^+\pi^-)=(8.53\pm0.69\pm0.64)\times10^{-5}$ and $\mathcal{B}(\eta'\to\pi^+\pi^-\pi^0\pi^0)=(1.82\pm0.35\pm0.18)\times10^{-4}$, which are in agreement with the predictions in Ref. [64], but not with an older estimate based on the broken-$SU(6)\times O(6)$ quark model [65].

3 Radiative and Dalitz decays

3.1 $\eta'\to\pi^+\pi^-\gamma$ [66]

The anomalous process $\eta'\to\gamma\pi^+\pi^-$ is the second most probable decay of the η' meson ($\mathcal{B}=29.1\pm0.5$) % [17]) and is frequently used for η' tagging. In the VMD model the main contribution to the decay comes from $\eta'\to\gamma\rho^0$ [67]. In the past the di-pion mass distribution was studied by several experiments *e.g.* JADE [68], CELLO [69], PLUTO [70], TASSO [71], TPC/$\gamma\gamma$ [72], and ARGUS [73]. A peak shift of about +20 MeV with respect to the expected position from the ρ^0 contribution was consistently observed. A dedicated [74] analysis using $\sim$2000 $\eta'\to\gamma\pi^+\pi^-$ events concluded that the ρ^0 contribution is not sufficient to describe the di-pion mass spectrum. This discrepancy could be attributed to the WZW box anomaly contribution, which should be included as an extra non-resonant term in the decay amplitude. It was suggested that the fits to the shape of the di-pion distribution will allow determination of the ratio of the two contributions [75]. Evidence for the box anomaly with a significance of 4σ was reported in 1997 by the Crystal Barrel experiment [76] using a sample of 7490$\pm$180 η' events, but this observation was not confirmed by a subsequent measurement by the L3 Collaboration [77] using 2123$\pm$53 events. A recently proposed model-independent approach, based on ChPT and a dispersion theory, describes the $\eta/\eta'\to\pi^+\pi^-\gamma$ decay amplitudes as a product of a universal and a reaction specific part [78]. The universal part could be extracted from the pion vector form factor measured precisely in $e^+e^-\to\pi^+\pi^-$. The reaction specific part was determined experimentally for the $\eta\to\pi^+\pi^-\gamma$ decay by WASA-at-COSY [79] and KLOE [80]. It was shown that the di-pion

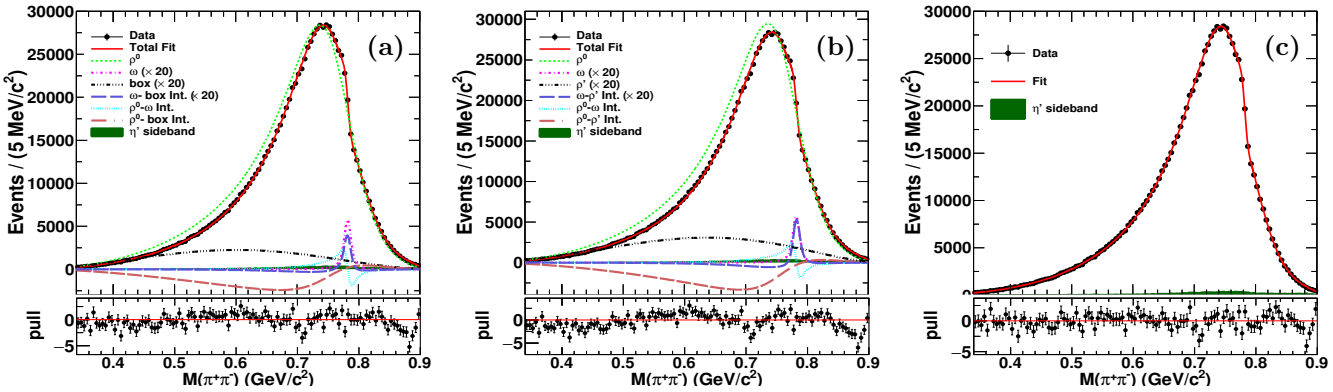

Fig. 12. (color online) The results of the model-dependent fits to $M(\pi^+\pi^-)$ with (a) $\rho^0-\omega-box\ anomaly$ and (b) $\rho^0-\omega-\rho^0(1450)$. (c) The results of the model-independent fit with ω interference.

distribution for the η decay cannot be described by the pion vector form factor only. In Ref. [81] it was hypothesized that the reaction specific part could be similar for η and η' decays.

For BESIII analysis a low background data sample of 9.7×10^5 $\eta'\to\gamma\pi^+\pi^-$ decays candidates is selected. The distribution of the $\pi^+\pi^-$ invariant mass, $M(\pi^+\pi^-)$, is displayed in Fig. 12. The $\rho^0-\omega$ interference is seen for the first time in this decay. In the model-dependent approach the data cannot be described with the Gounaris-Sakurai parameterisation [82] of the ρ^0 and the ω contributions including the interference. The fit performance gets much better after including the box anomaly, Fig. 12(a), with a statistical significance larger than 37σ. An alternative fit was performed by replacing the box anomaly with $\rho^0(1450)$, Fig. 12(b), by fixing its mass width to the world average values. The fit is slightly worse but it still provides a reasonable description of the data.

Using the model-independent approach of Ref. [78] and including $\rho^0-\omega$ mixing, the pion vector form factor $F_V(s)$ (where $s=M^2(\pi^+\pi^-)$) and amplitudes for $\eta/\eta'\to\gamma\pi^+\pi^-$ decays are proportional to $P(s)\cdot\Omega(s)$, where $P(s)$ is a reaction-specific term, $P(s)=1+\kappa s+\lambda s^2+\xi\cdot BW_\omega+\mathcal{O}(s^4)$,and $\Omega(s)$ is the Omnes function describing $\pi-\pi$ interactions with $L=1$ [81, 83]. For $\eta\to\gamma\pi^+\pi^-$ only the linear term $\kappa=1.32\pm0.13$ GeV^{-2} [79, 80] is needed. The fit to the BESIII $\eta'\to\gamma\pi^+\pi^-$ data is shown in Fig. 12(c). It yields $\kappa=0.992\pm0.039\pm0.067\pm0.163$ GeV^{-2}, $\lambda=-0.523\pm0.039\pm0.066\pm0.181$GeV^{-4}, and $\xi=0.199\pm0.006\pm0.011\pm0.007$, where the first uncertainties are statistical, the second are systematic, and the third are theoretical. The presence of the quadratic term is consistent with recent calculations including an intermediate $\pi^\pm a_2^\mp$ state [84].

3.2 $\eta'\to\pi^+\pi^-l^+l^-$ [85]

The first observation of the conversion decay $\eta'\to\pi^+\pi^-e^+e^-$ was reported in 2009 by the CLEO [63] collaboration. The decay is directly related to $\eta'\to\pi^+\pi^-\gamma$ and involves a virtual photon, $\eta'\to\pi^+\pi^-\gamma^*\to\pi^+\pi^-e^+e^-$. The conversion process provides a more stringent test of the models. Predictions for the decay are given within the VMD model and unitarized ChPT [86–88]. In the e^+e^- invariant mass ($q\equiv M(e^+e^-)$) distribution for a conversion decay, the contribution of the photon propagator translates to the pole-like $1/q$ dependence close to the lower kinematic boundary of $q=2m_e$ (see also Sec. **3.3**). For the $\eta'\to\pi^+\pi^-e^+e^-$ decay a dominant ρ^0 contribution in $M(\pi^+\pi^-)$ is also expected. The CLEO measurement based on just $7.9^{+3.9}_{-2.7}$ signal events was unable to explore these distributions. However, the measured branching fraction $\mathcal{B}(\eta'\to\pi^+\pi^-e^+e^-)=(2.5^{+1.2}_{-0.9}\pm0.5)\times10^{-3}$ [63], is consistent with the predicted value of $\sim2\times10^{-3}$. The corresponding conversion decay with a $\mu^+\mu^-$ pair is suppressed by two orders of magnitude due to the $q=2m_\mu$ cutoff. In the CLEO analysis an upper limit of $\mathcal{B}(\eta'\to\pi^+\pi^-\mu^+\mu^-)<2.4\times10^{-4}$, at 90% C.L. was set.

The completed BESIII analysis is based only on 2009 data. Figure 13 displays the e^+e^- mass spectrum from requiring $|M(\pi^+\pi^-e^+e^-)-m_{\eta'}|<0.02$ GeV/c^2, where the background from $\gamma\pi^+\pi^-$ following the photon conversion in the detector material can be clearly seen. The peak close to $2m_e$ corresponds to the $\eta'\to\pi^+\pi^-e^+e^-$ signal and the second peak around 0.015 GeV/c^2 comes from the $\eta'\to\gamma\pi^+\pi^-$ background. For the selected data sample any other background is negligible and the efficiency for the signal is 16.9%. The number of 429 ± 24 signal events is taken from a fit of the two contributions to the $M(e^+e^-)$ distribution. The corresponding branching fraction of $\mathcal{B}(\eta'\to\pi^+\pi^-e^+e^-)=(2.11\pm0.12\pm0.15)\times10^{-3}$ is in good agreement with theoretical predictions and with the CLEO result. The mass spectra of $\pi^+\pi^-$ and e^+e^- are consistent with the expected ρ^0 dominance in the $M(\pi^+\pi^-)$ distribution and the long-tailed peak in the $M(e^+e^-)$ distribution just above the $2m_e$ threshold.

Figure 14 shows the invariant mass of $\pi^+\pi^-\mu^+\mu^-$, where no η' signal is observed. The remaining events in

the η' mass region are consistent with the contributions from the background estimated with MC simulations. An upper limit of $\mathcal{B}(\eta'\to\pi^+\pi^-\mu^+\mu^-)<2.9\times10^{-5}$ at the 90% C.L. is set.

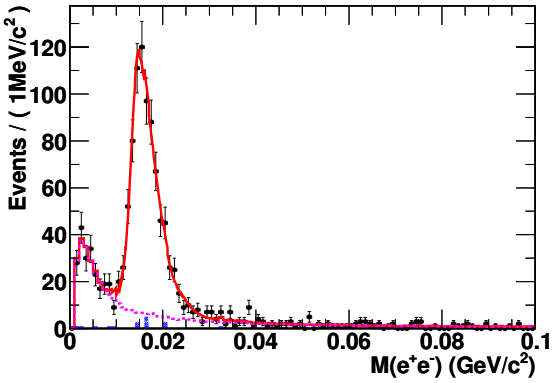

Fig. 13. (color online) The invariant mass spectrum of e^+e^- for data (dots with error bars). The solid line represents the fit result, the dotted histogram is the MC signal shape and the shaded histogram is for backgrounds obtained from η' sideband events. Reprinted figure with permission from M. Ablikim et al, Phys. Rev. D 87, 092011, 2013 (DOI: https://doi.org/10.1103/PhysRevD.87.092011) (Ref. [85]). Copyright 2013 by the American Physical Society.

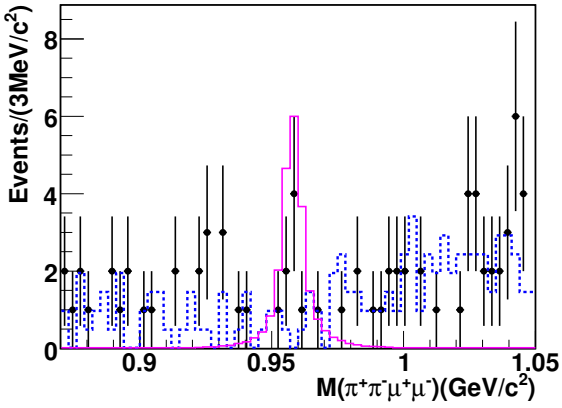

Fig. 14. (color online) Invariant mass spectrum of $\pi^+\pi^-\mu^+\mu^-$ for data (dots with error bars). The solid line represents the fit result, the dotted histogram is the MC signal shape and the shaded histogram is for backgrounds obtained from η' sideband events. Reprinted figure with permission from M. Ablikim et al, Phys. Rev. D 87, 092011, 2013 (DOI: https://doi.org/10.1103/PhysRevD.87.092011) (Ref. [85]). Copyright 2013 by the American Physical Society.

3.3 $\eta'\to\gamma e^+e^-$ [12]

Dalitz decays of light pseudoscalar mesons, $P\to\gamma e^+e^-$ where $P=\pi^0$, η, η', play an important role in revealing the structure of the hadrons and the interaction mechanism between photons and the hadrons [9]. The decay rates can be calculated in quantum electrodynamics (QED) where the inner structure of the mesons is encoded by the transition form factor (TFF), $F(q^2)$, where q^2 is the invariant mass of the lepton pair squared. A recent summary and discussion of this subject can be found in Ref. [89].

Knowledge of the TFF is also important in studies of the muon anomalous magnetic moment, $a_\mu=(g_\mu-2)/2$, which is one of the most precise low-energy tests of the SM and an important probe for new physics. The theoretical uncertainty in the SM calculation of a_μ is dominated by hadronic corrections and therefore limited by the accuracy of their determination [90]. In particular, the hadronic light-by-light (HLbL) scattering contribution to a_μ includes two meson-photon-photon vertices that can be related to the TFF. Thus, models describing these transitions should be tested to reduce the uncertainty in the SM prediction for a_μ.

The conversion decay $\eta'\to\gamma e^+e^-$ is closely related to $\eta'\to\gamma\pi^+\pi^-$, and in particular the transition form factor could be predicted from the invariant mass distribution of the two pions and the branching ratio of the $\eta'\to\gamma\pi^+\pi^-$ decay in a model independent way using a dispersive integral [81].

The differential decay width [9] is calculated with,

$$\frac{\mathrm{d}\Gamma(\eta'\to\gamma l^+l^-)}{\mathrm{d}q^2\Gamma(\eta'\to\gamma\gamma)}=[\mathrm{QED}(q^2)]\times|F(q^2)|^2, \tag{5}$$

where $[\mathrm{QED}(q^2)]$ represents the QED part for a point-like meson which includes a $1/q^2$ term due to the photon propagator. Therefore, for conversion decays involving an electron-positron pair, the distribution peaks at the lowest invariant masses $q=2m_e$. The TFF can be experimentally determined from the ratio of the measured dilepton invariant mass spectrum and the $[\mathrm{QED}(q^2)]$ term. In the VMD model, it is assumed that interactions between virtual photon and hadrons are described by a superposition of neutral vector meson states [8, 91]. The dominant contribution is expected to come from the ρ^0 meson and the form factor can be described by:

$$F(q^2)=N\frac{m_V^2}{m_V^2-q^2-\mathrm{i}\Gamma_V m_V}, \tag{6}$$

where N is a factor ensuring that $F(0)=1$ and $m_V\approx m_\rho$, $\Gamma_V\approx\Gamma_\rho$ where m_ρ, Γ_ρ is the mass and width of the ρ^0 meson respectively. In the case of the η', the mass of the pole lies within the kinematic boundaries of the decay and therefore the $-\mathrm{i}\Gamma_V m_V$ term cannot be neglected. A

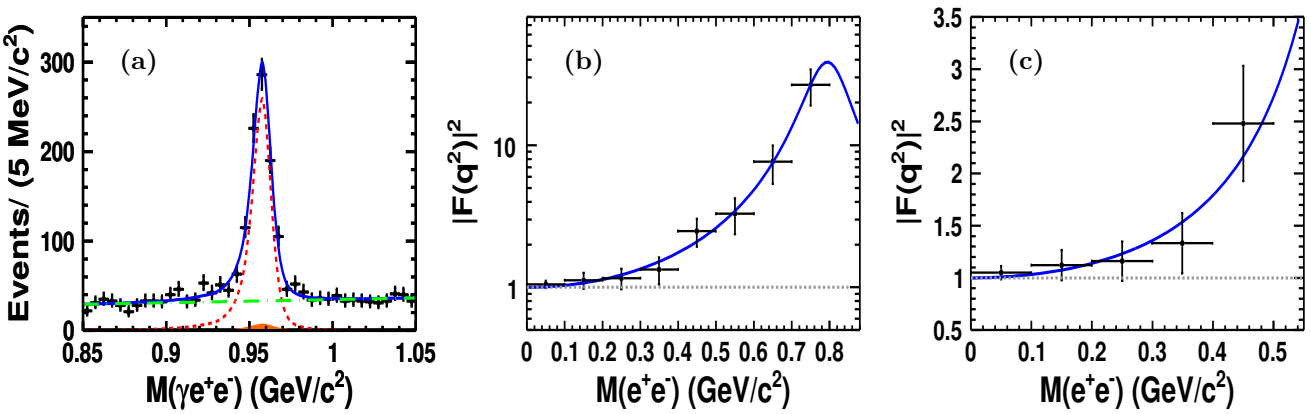

Fig. 15. (color online) (a) Invariant γe^+e^- mass distribution for the selected signal events. The (black) crosses are the data, the (red) dashed line represents the signal, the (green) dot-dashed curve shows the non-peaking background shapes, and the (orange) shaded component is the shape of the peaking background events. (b) Fit to the single pole form factor $|F|^2$. (c) Determination of the form factor slope by fitting to $|F|^2$. Reprinted figures with permission from M. Ablikim et al, Phys. Rev. D 92, 012001, 2015 (DOI: https://doi.org/10.1103/PhysRevD.92.012001) (Ref. [12]). Copyright 2015 by the American Physical Society.

parameter often extracted experimentally is the slope of the form factor, b, defined as

$$b=\left.\frac{\mathrm{d}|F|}{\mathrm{d}q^2}\right|_{q^2=0}=\frac{1}{m_V^2+\Gamma_V^2}. \quad (7)$$

Before the BESIII result, only the $\eta'\to\gamma\mu^+\mu^-$ process had been observed, with the TFF slope measured to be $b_{\eta'}=(1.7\pm0.4)$ GeV^{-2} [9, 92]. In the VMD model, $\Gamma(\eta'\to\gamma e^+e^-)/\Gamma(\eta'\to\gamma\gamma)=(2.06\pm0.02)\%$ [88], to be compared to 1.8% if the TFF is set to one. The TFF slope is expected to be $b_{\eta'}=1.45$ GeV^{-2} [93, 94] in the VMD model, while in ChPT it is $b_{\eta'}=1.60$ GeV^{-2} [95]. A recent calculation based on a dispersion integral gives $b_{\eta'}=1.53^{+0.15}_{-0.08}$ GeV^{-2} [81].

In the BESIII experiment the largest background comes from QED processes and $J/\psi\to e^+e^-\gamma\gamma$ decays. For these channels, the combination of the e^+e^- with any final-state photon produces a smooth $M(\gamma e^+e^-)$ distribution. The primary peaking background comes from the decay $\eta'\to\gamma\gamma$ followed by a γ conversion in the material in front of the main drift chamber. The distance from the reconstructed vertex point of the electron-positron pair to the z axis is used to reduce the background down to 42.7 ± 8.0 events. The resulting $M(\gamma e^+e^-)$ distribution after the selection criteria is shown in Fig. 15(a) and exhibits a clear peak at the η' mass. A fit is performed to determine the signal yield, with the signal shape represented by the MC. The non-peaking background is described by a first-order Chebychev polynomial. The fraction of the peaking background is fixed from the simulation. The signal yield and the detection efficiency is summarized in Table 2. The decay $\eta'\to\gamma\gamma$ from the same data set is used for normalization and the result is quoted in terms of the ratio $\Gamma(\eta'\to\gamma e^+e^-)/\Gamma(\eta'\to\gamma\gamma)=(2.13\pm0.09\pm0.07)\times10^{-2}$. Using the branching fraction of $\eta'\to\gamma\gamma$ in the PDG [17], we obtain the first measurement of the $\eta'\to\gamma e^+e^-$ branching fraction as reported in Table 2.

The TFF is extracted from the bin-by-bin efficiency corrected signal yields for eight $M(e^+e^-)$ bins for $M(e^+e^-)<0.80$ GeV/c^2. The bin widths of 0.1 GeV are used and are much wider than the $M(e^+e^-)$ resolution (5∼6 MeV depending on $M(e^+e^-)$). The signal yield in each $M(e^+e^-)$ bin is obtained by repeating the fits to the $M(\gamma e^+e^-)$ mass distributions.

The result for $|F|^2$ is obtained by dividing the acceptance corrected yields by the integrated QED prediction in each $M(e^+e^-)$ bin and it is shown in Figs. 15(b) and (c). The parameters from the fit of the TFF to the parametrization of Eq. 6 are $m_V=(0.79\pm0.04\pm0.02)$ GeV and $\Gamma_V=(0.13\pm0.06\pm0.03)$ GeV. The single pole parameterization provides a good description of data, as shown in Fig. 15(b). The corresponding value of the slope parameter is $b_{\eta'}=(1.56\pm0.19)$ GeV^{-2}, in agreement with the result from $\eta'\to\gamma\mu^+\mu^-$ [9]. The slope also agrees, within errors, with the VMD model predictions, and the uncertainty matches the best determination in the space-like region from the CELLO collaboration, $b_{\eta'}=(1.60\pm0.16)$ GeV^{-2} [96].

3.4 $\eta'\to e^+e^-\omega$ [13]

The decay $\eta'\to\pi^+\pi^-e^+e^-$ [85] is dominated by $\eta'\to\rho^0e^+e^-$, in agreement with theoretical predictions [86, 87]. The corresponding decay $\eta'\to\omega e^+e^-$ was not observed before the BESIII measurements. Theoretical models [86, 97] predict the branching fraction to be around 2.0×10^{-4}.

A parallel analysis of $\eta'\to e^+e^-\omega$ and $\eta'\to\gamma\omega$ decays

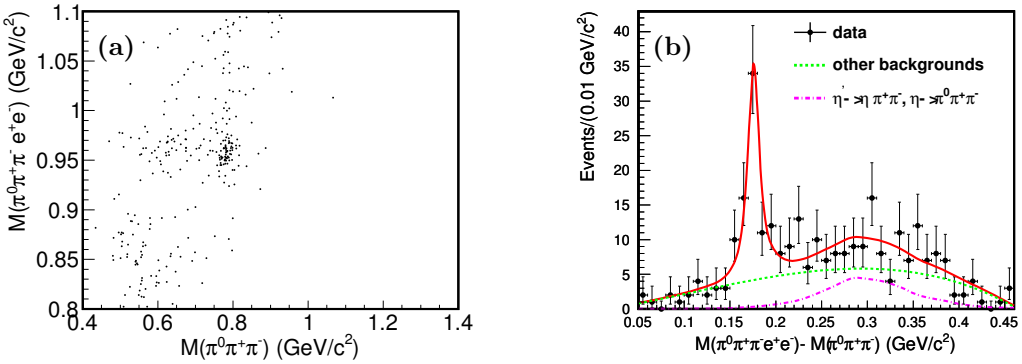

Fig. 16. (color online) (a) Distribution of $M(\pi^0\pi^+\pi^-e^+e^-)$ versus $M(\pi^0\pi^+\pi^-)$. (b) Distribution of $M(\pi^0\pi^+\pi^-e^+e^-)-M(\pi^0\pi^+\pi^-)$ with the fit results. The dash-dotted line is the $\eta'\to\pi^+\pi^-\eta$ background contributions and the dotted line is the remaining background. Reprinted figures with permission from M. Ablikim et al, Phys. Rev. D 92, 051101(R), 2015 (DOI: https://doi.org/10.1103/PhysRevD.92.051101) (Ref. [13]). Copyright 2015 by the American Physical Society.

allows reduction of the impact of systematic errors for the ratio of the branching fractions. For $\eta'\to e^+e^-\omega$ decays, candidate events with four well-reconstructed charged tracks and at least three photons are selected. The external conversion background from $\eta'\to\gamma\omega$ is removed by requiring the distance of the vertex from the z axis to be less than 2 cm (according to simulation only 2.6±0.3 background events will survive the cut). In the selected data sample both the ω peak in $M(\pi^0\pi^+\pi^-)$ and the η' peak in $M(\pi^0\pi^+\pi^-e^+e^-)$ are clearly seen in the scatter plot shown in Fig. 16(a). The best identification of the process is achieved in the $M(\pi^0\pi^+\pi^-e^+e^-)$–$M(\pi^0\pi^+\pi^-)$ distribution. This distribution is used in a fit to extract the signal yields as indicated in Fig. 16(b). The decay of $\eta'\to\omega e^+e^-$ is observed with a statistical significance of 8σ, and its branching fraction is measured to be $\mathcal{B}(\eta'\to\omega e^+e^-)=(1.97\pm0.34\pm0.17)\times10^{-4}$, consistent with theoretical predictions [86, 97].

3.5 $\eta'\to\gamma\gamma\pi^0$ [14]

The $\eta'\to\gamma\gamma\pi^0$ decay should be dominated by the sequential process $\eta'\to\gamma\omega\to\gamma\gamma\pi^0$. The interesting question is to determine a non-resonant contribution to the decay. At present there is only a preliminary theoretical analysis which uses a combination of the linear sigma model and VMD. The prediction for the branching fraction of $\eta'\to\gamma\gamma\pi^0$ is $\sim6\times10^{-3}$ [98, 99]. This is quite a puzzling result, giving a value two times larger than the $\gamma\omega$ sequence. The first observation of $\eta'\to\gamma\gamma\pi^0$ was reported by the BESIII experiment. Figure 17(a) shows the $\gamma\gamma\pi^0$ invariant mass spectrum, where the clear η' peak is observed. By assuming that the inclusive decay $\eta'\to\gamma\gamma\pi^0$ can be attributed to the vector mesons ρ^0 and ω and the non-resonant contribution, an unbinned maximum likelihood fit to the $\gamma\pi^0$ invariant mass (Fig. 17(b)) is performed to determine the signal yields for the non-resonant $\eta'\to\gamma\gamma\pi^0$ decay using the η' signal events with $|M(\gamma\gamma\pi^0)-m_{\eta'}|<25$ MeV/c^2. In the fit, the ρ^0-ω interference is considered, but possible interference between the ω (ρ^0) and the non-resonant process is neglected.

The branching fraction of the inclusive decay is measured to be $\mathcal{B}(\eta'\to\gamma\gamma\pi^0)_{\rm Incl.}=(3.20\pm0.07\pm0.23)\times10^{-3}$, which is much lower than the theoretical predictions [98, 99]. In addition, the branching fraction for the non-resonant decay is determined to be $\mathcal{B}(\eta'\to\gamma\gamma\pi^0)_{\rm NR}=(6.16\pm0.64\pm0.67)\times10^{-4}$, which agrees with the upper limit measured by the GAMS-2000 experiment [59]. As a validation of the fit, the product branching fraction with the omega intermediate state involved is obtained to be $\mathcal{B}(\eta'\to\gamma\omega)\cdot\mathcal{B}(\omega\to\gamma\pi^0)=(2.37\pm0.07\pm0.18)\times10^{-3}$, which is consistent with the PDG value [17]. Hopefully this first result will trigger new theory analyses of the decay. In particular, a combined analysis of this decay with $\eta'\to\pi^+\pi^-\pi^0\gamma$ might provide more details about the roles of isoscalar mesons and isospin violating processes in the η' transition form factor.

4 Rare decays

4.1 Invisible decays [100]

Studies of η and η' decays where one or more of the products escapes detection is a sensitive probe for new light particles beyond the SM. A two-body hadronic decay $J/\psi\to\phi\eta(\eta')$ is well suited to tag production of η/η' mesons, since the presence of undetected particles could be established from missing four-momentum. The ϕ meson is reconstructed efficiently and with good resolution from the K^+K^- decay. This method was first applied for searches for the invisible decays of η/η' (*i.e.* where none of the decay products is observed) at the BESII experiment in 2005 [101].

At BESIII the search for the invisible decays of η

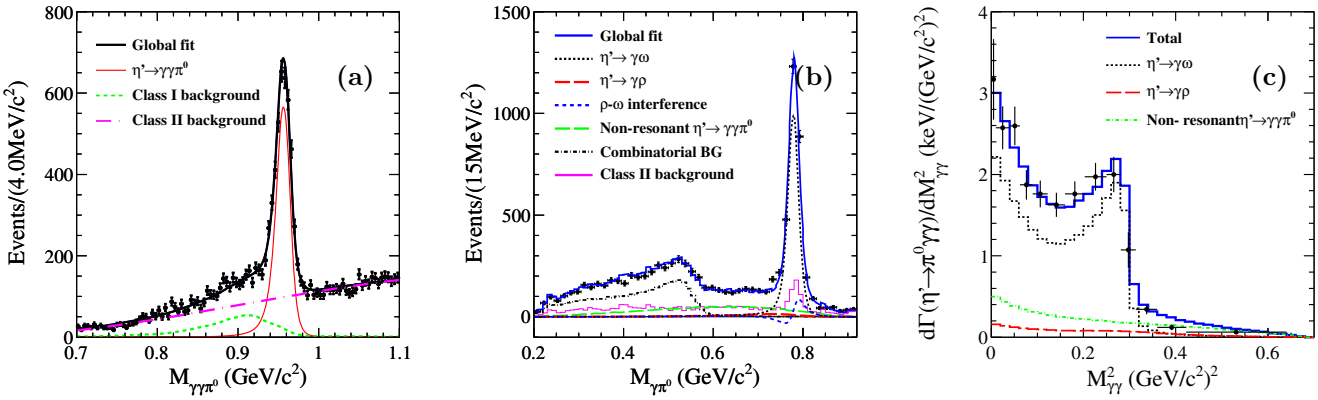

Fig. 17. (color online) (a) Distribution of $M(\gamma\gamma\pi^0)$ for the selected inclusive $\eta'\to\gamma\gamma\pi^0$ signal events. The dotted and dot-dashed curves are background contributions. The total fit result is shown as the solid line. (b) Distribution of $M(\gamma\pi^0)$ and fit result (solid line). The dotted curve is the ω-contribution; the long dashed-curve the ρ^0-contribution; and the short dashed-curve is the ρ^0-ω interference. (c) Acceptance corrected and normalized to the partial width (in keV) $M^2(\gamma\gamma)$ distribution for the inclusive $\eta'\to\gamma\gamma\pi^0$ decay. The error includes the statistic and systematic uncertainties. The (blue) histogram is the incoherent sum of ρ^0 and ω and the non-resonant components from MC simulations; the (black) dotted curve is the ω-contribution; the (red) dot-dashed curve is the ρ^0-contribution; and the (green) dashed curve is the non-resonant contribution. Reprinted figure with permission from M. Ablikim et al, Phys. Rev. D 96, 012005, 2017 (DOI: https://doi.org/10.1103/PhysRevD.96.012005) (Ref. [14]). Copyright 2017 by the American Physical Society.

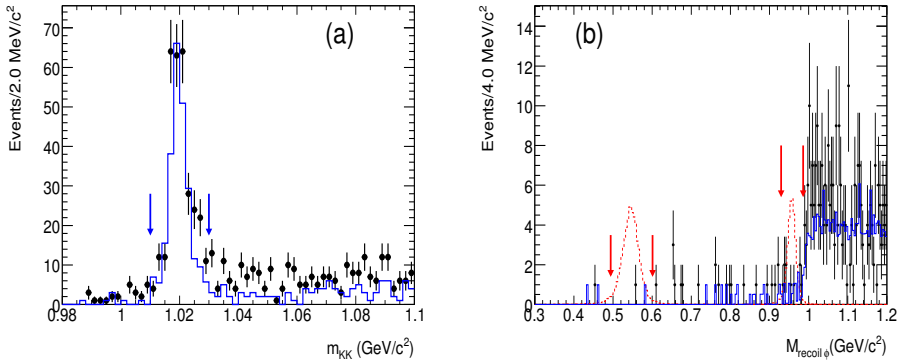

Fig. 18. (color online) (a) $M(\mathrm{K^+K^-})$ distribution. (b) Recoil mass distribution against ϕ candidates, M_ϕ^{recoil}. Points with error bars are data; the (blue) solid histogram is the sum of the expected backgrounds; the dashed histograms (with arbitrary scale) are signals of η and η' invisible decays from MC simulations; and the arrows on the plot indicate the signal regions of the η and $\eta'\to$*invisible* decays. Reprinted figure with permission from M. Ablikim et al, Phys. Rev. D 87, 012009, 2013 (DOI: https://doi.org/10.1103/PhysRevD.87.012009) (Ref. [100]). Copyright 2013 by the American Physical Society.

and η' was repeated using the 2009 data set *i.e.* with statistics four times larger than BESII. The event selection requires exactly two tracks with opposite charges, identified as kaons. Figure 18(a) shows the invariant mass of the kaons, $M(\mathrm{K^+K^-})$, with a clear ϕ peak, while no evident η or η' signal is observed in the mass spectrum for the ϕ recoil system as shown in Fig. 18(b). To reduce the systematic uncertainty, the $\eta(\eta')\to\gamma\gamma$ decay is also identified in $J/\psi\to\phi\eta(\eta')$, and the ratios of $\mathcal{B}(\eta(\eta')\to\text{invisible})$ to $\mathcal{B}(\eta(\eta')\to\gamma\gamma)$ are determined. Using the world averages [17] for the two photon branching fractions of η and η', the following 90% C.L. upper limits are obtained: $\mathcal{B}(\eta\to\text{invisible})<1.32\times10^{-4}$ and $\mathcal{B}(\eta'\to\text{invisible})<5.31\times10^{-4}$.

4.2 $\eta/\eta'\to\pi^+e^-\bar{\nu}_e+c.c.$ [102]

Within the framework of chiral perturbation theory, the upper bound of the branching fraction $\eta\to\pi^+l^-\bar{\nu}_l$ is predicted to be 2.6×10^{-13}. After considering scalar or vector type interaction, the branching fraction of $\eta\to\pi^+l^-\bar{\nu}_l$ was estimated to be $10^{-8}-10^{-9}$ [103, 104], which is a few orders of magnitudes higher than that in the SM. Therefore, searches for the $\eta\to\pi^+l^-\bar{\nu}_l$ and $\eta'\to\pi^+l^-\bar{\nu}_l$ at the branching fractions level of 10^{-8}–10^{-9}

and below will provide information on new physics beyond the SM.

At BESIII, searches for the decays of η and $\eta' \to \pi^+e^-\bar{\nu}_e$+c.c. were performed using $J/\psi \to \phi\eta$ and $\phi\eta'$ with the ϕ meson reconstructed using K^+K^- decay. No signals are observed in the $\pi^+e^-\bar{\nu}_e$ mass spectrum shown in Fig. 19 for either η or η', and upper limits at the 90% C.L. are determined to be 7.3×10^{-4} and 5.0×10^{-4} for the ratios $\mathcal{B}(\eta\to\pi^+e^-\bar{\nu}_e$+c.c.$)/\mathcal{B}(\eta\to\pi^+\pi^-\pi^0)$ and $\mathcal{B}(\eta'\to\pi^+e^-\bar{\nu}_e$+c.c.$)/\mathcal{B}(\eta'\to\pi^+\pi^-\eta)$, respectively. Using the known values of $\mathcal{B}(\eta\to\pi^+\pi^-\pi^0)$ and $\mathcal{B}(\eta'\to\pi^+\pi^-\eta)$, the 90% C.L. upper limits for the semileptonic decay rates are $\mathcal{B}(\eta \to \pi^+e^-\bar{\nu}_e$+c.c.$) < 1.7\times10^{-4}$ and $\mathcal{B}(\eta' \to \pi^+e^-\bar{\nu}_e$+c.c.$)<2.2\times10^{-4}$.

4.3 $\eta/\eta'\to\pi\pi$ [105]

In the SM, these processes can proceed via the weak interaction with a branching fraction of order 10^{-27}, according to Ref. [106]. Higher branching fractions are possible either by introducing a CP violating term in the QCD Lagrangian (a branching fraction up to 10^{-17} can be obtained in this scheme) or allowing CP violation in the extended Higgs sector (with $\mathcal{B}$ up to 10^{-15}), as described in Ref. [106]. The detection of these decays at any level accessible today would signal P and CP violations from new sources, beyond any considered extension of the SM. In BESIII analysis of the 2009 data set, CP and P violating decays of $\eta/\eta' \to \pi^+\pi^-$ and $\pi^0\pi^0$ were searched for in J/ψ radiative decays. The mass spectra of $\pi^+\pi^-$ and $\pi^0\pi^0$ are shown in Fig. 20 and Fig. 21, respectively. No significant η or η' signal is observed. Using the Bayesian method, the 90% C.L. upper limits are determined to be $\mathcal{B}(\eta \to \pi^+\pi^-) < 3.9\times10^{-4}$, $\mathcal{B}(\eta' \to \pi^+\pi^-) < 5.5\times10^{-5}$, $\mathcal{B}(\eta \to \pi^0\pi^0) < 6.9\times10^{-4}$ and $\mathcal{B}(\eta'\to\pi^0\pi^0)<4.5\times10^{-4}$.

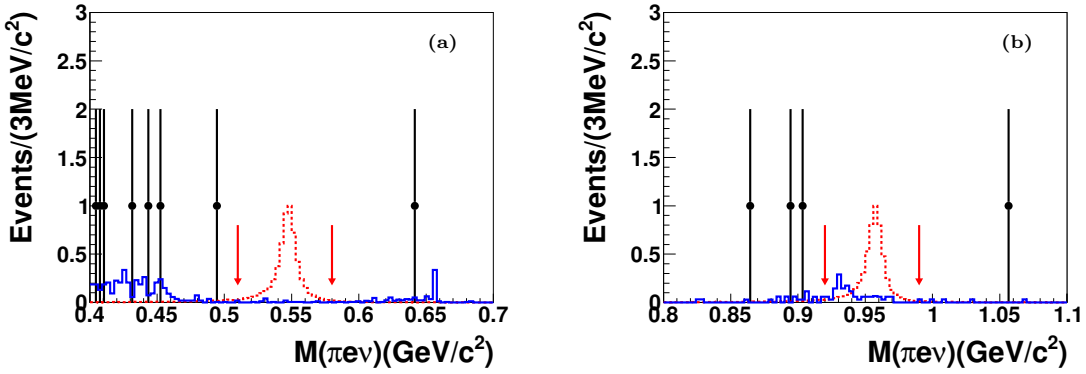

Fig. 19. (color online)The $M(\pi^+e^-\bar{\nu}_e)$ distributions of candidate events: (a) for $J/\psi\to\phi\eta$ ($\eta\to\pi^+e^-\bar{\nu}_e$); (b) for $J/\psi\to\phi\eta'$ ($\eta'\to\pi^+e^-\bar{\nu}_e$). For both (a) and (b): the data (dots with error bars) are compared to the signal MC samples (red dashed histogram) and the expected backgrounds (solid blue histogram). The arrows on the plots indicate the signal regions of η and η' candidates. Reprinted figure with permission from M. Ablikim et al, Phys. Rev. D 87, 032006, 2013 (DOI: https://doi.org/10.1103/PhysRevD.87.032006) (Ref. [102]). Copyright 2013 by the American Physical Society.

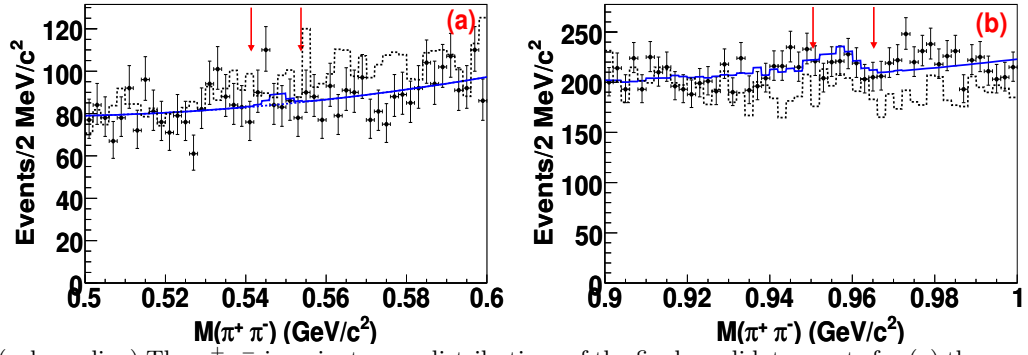

Fig. 20. (color online) The $\pi^+\pi^-$ invariant mass distributions of the final candidate events for (a) the η mass region, and (b) the η' mass region. The dots with error bars are data, the solid lines are the fit described in the text, and the dashed histograms are the sum of all the simulated normalized backgrounds. Reprinted figure with permission from M. Ablikim et al, Phys. Rev. D 84, 032006, 2011 (DOI: https://doi.org/10.1103/PhysRevD.84.032006) (Ref. [105]). Copyright 2011 by the American Physical Society.

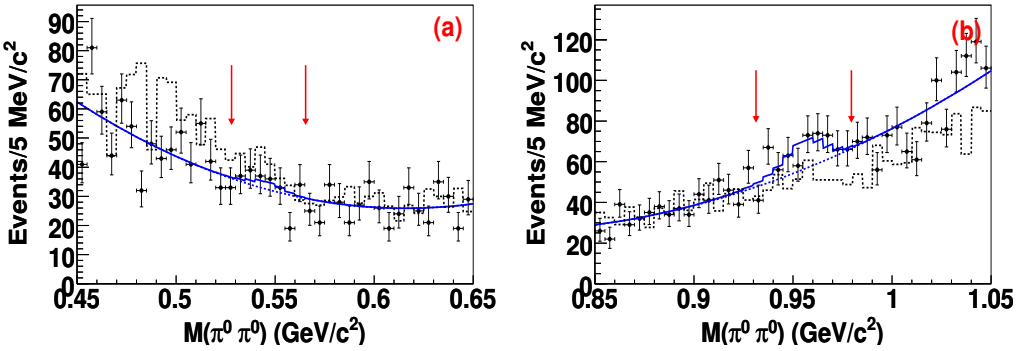

Fig. 21. (color online) The $\pi^0\pi^0$ invariant mass distributions of the final candidate events for (a) the η mass region, and (b) the η' mass region. The dots with error bars are the data, the solid lines are the fit described in the text, and the dashed histograms are the sum of all the simulated normalized backgrounds. Reprinted figure with permission from M. Ablikim et al, Phys. Rev. D 84, 032006, 2011 (DOI: https://doi.org/10.1103/PhysRevD.84.032006) (Ref. [105]). Copyright 2011 by the American Physical Society.

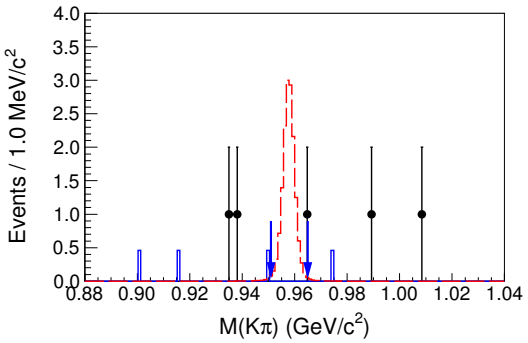

Fig. 22. (color online) The $K^{\pm}\pi^{\mp}$ invariant mass distribution, where the arrows show the signal region. The dots with error bars are the data, the dashed histogram is for the signal MC with arbitrary normalization, and the solid histogram is the background contamination from a MC simulation of $J/\psi \to \phi\pi^+\pi^-$. Reprinted figure with permission from M. Ablikim et al, Phys. Rev. D 93, 072008, 2016 (DOI: https://doi.org/10.1103/PhysRevD.93.072008) (Ref. [107]). Copyright 2016 by the American Physical Society.

4.4 $\eta' \to K^{\pm}\pi^{\mp}$ [107]

Non-leptonic weak decays are valuable tools for exploring physics beyond the SM. Among the non-leptonic decays, the decay $\eta' \to K^{\pm}\pi^{\mp}$ is of special interest due to the long-standing problem of the $\Delta I = 1/2$ rule in weak non-leptonic interactions. The branching fraction of the $\eta' \to K^{\pm}\pi^{\mp}$ decay is predicted to be of the order of $10^{-10} \sim 10^{-11}$ [108, 109], with a large long-range hadronic contribution expected.

A search for the non-leptonic weak decay $\eta' \to K^{\pm}\pi^{\mp}$ is performed for the first time through the $J/\psi \to \phi\eta'$ decay, while no evidence for $\eta' \to K^{\pm}\pi^{\mp}$ is seen in the $K\pi$ mass spectrum (Fig. 22). Thus the 90% C.L. upper limit on $\mathcal{B}(\eta' \to K^{\pm}\pi^{\mp})$ of 3.8×10^{-5} is reported.

5 Summary

J/ψ decays provide a clean source of η' for decay studies. Based on the world's largest sample of J/ψ events, the recent results on η/η' decays achieved at the BESIII experiment are presented. In addition to the improved accuracy of the branching fractions of η', observations of η' new decay modes, including $\eta' \to \pi^+\pi^-\pi^+\pi^-$, $\eta' \to \pi^+\pi^-\pi^0\pi^0$, $\eta' \to \rho^{\mp}\pi^{\pm}$ and $\eta' \to \gamma e^+e^-$, have been reported for the first time. The precision of the $\eta' \to \pi^+\pi^-\gamma$ $M(\pi^+\pi^-)$ distribution from BESIII with clear $\rho^0-\omega$ interference is comparable to the $e^+e^- \to \pi^+\pi^-$ data and allows comparison of these two reactions in both model dependent and model independent ways. In particular a competitive extraction of the $\omega \to \pi^+\pi^-$ branching fraction is possible. It is found that an extra contribution is necessary to describe the data besides the contributions from $\rho^0(770)$ and ω.

Despite the impressive progress, many η/η' decays are still to be observed and explored. The BESIII detector will collect a sample of 10^{10} J/ψ events in the near future, thus making further more detailed η/η' studies possible. The statistical uncertainty will be reduced significantly and the challenge will be to reduce the systematic uncertainties which will dominate the precision of many η/η' decay measurements. Such reduction could be achieved by optimization of the particle identification, photon detection and charged particle tracking methods, by detailed consistency checks of the MC simulations, and by use of control data sets to adjust the simulations.

A list of the specific decay channels where the new data is expected to have an important impact includes:

1) Larger data samples of $\eta \to \pi^+\pi^-\pi^0$ and $\eta \to \pi^0\pi^0\pi^0$ decays from the BESIII experiment are needed to provide independent checks of the analyses carried out at other experiments. The Dalitz plot distributions will be made available for the direct fits to theory. In particular, data from the planned run will allow collection of

approximately 0.5×10^6 events of $\eta\to\pi^+\pi^-\pi^0$ with negligible background. In addition, one could probably also use other J/ψ decay modes as sources of η mesons. Some possible examples are $J/\psi\to\omega\eta$ ($\mathcal{B}=(1.74\pm0.20)\times10^{-3}$) and $J/\psi\to p\bar{p}\eta$ ($\mathcal{B}=(2.00\pm0.12)\times10^{-3}$).

2) For $\eta'\to\pi^+\pi^-\eta$ and $\eta'\to\pi^0\pi^0\eta$ decays the analysis could be extended not only by using the new data but also by reconstructing the final states with three pion decay modes of η in addition to $\eta\to\gamma\gamma$. The increased statistics would allow *e.g.* to search for the cusp in $\eta'\to\pi^0\pi^0\eta$ and provide further information about $\eta\pi$ scattering [57]. In addition, the use of the same final state topology $\eta'\to\pi^+\pi^-(\eta\to\pi^0\pi^0\pi^0)$ and $\eta'\to\pi^0\pi^0(\eta\to\pi^+\pi^-\pi^0)$ will enable determination of the ratio of the two decay modes with low systematic uncertainty.

3) For $\eta'\to\pi^0\pi^0\pi^0$ and $\eta'\to\pi^+\pi^-\pi^0$, larger statistics are crucial to carry out amplitude analysis of the processes. At present it is impossible to differentiate between S and D waves. A detailed understanding of this process dynamics is a prerequisite for a program of light quark mass determination from comparison with the $\eta'\to\pi\pi\eta$ processes, a method which does not rely on the full decay width value. Several theory groups have expressed interest in description of the decay within a dispersive approach. The overall goal is understanding of all parity-even processes of η and η'.

4) The hadronic parity-odd processes $\eta'\to\pi^+\pi^-\pi^+\pi^-$, $\pi^+\pi^-\pi^0\pi^0$ offer a window to study the double off-shell transition form factor of η'. The ultimate goal would be to carry out amplitude analysis of the reactions. The new data, with about 1200 events expected, would allow for the first stage of such an analysis. However, the collected data on these decays, together with the $\eta'\to\pi^+\pi^-e^+e^-$ decay, will already provide unique constraints and checks for the models of the η' double off-shell transition form factor. In addition, since the predicted branching fraction for the related $\eta'\to\pi^+\pi^-\mu^+\mu^-$ process is about 2×10^{-5}, the decay will likely be observed with the new data. The branching fraction value of this decay is sensitive to the η' transition form factor.

5) For the $\eta'\to\pi^+\pi^-e^+e^-$ decay much progress is expected. A combined analysis of the 2012 data and the new run data will allow for a sample close to 2×10^4 events. In particular a CP symmetry test by measurement of asymmetry between the lepton and the pion decay planes [110, 111], as well as studies of the $M(e^+e^-)$ and $M(\pi^+\pi^-)$ distributions, would be possible.

6) Among the very rare decays of η/η' discussed in this review, the largest impact of the new data is expected for the invisible decays, $\eta/\eta'\to\pi^+e^-\bar{\nu}_e$ and $\eta'\to K^\pm\pi^\mp$, where no background is observed. Therefore the sensitivity should scale with luminosity. In addition, the results for the first two decay modes are based on the 2009 data set only.

Both η and η' decays are important tools for studies of strong interactions in the non-perturbative region and for determination of some SM parameters. In addition, they provide an indirect way to probe physics beyond the SM. In particular, the η and η' decay program pursued at BESIII, where the data collected at J/ψ are used for a wealth of other studies, is a smart and resource-efficient research strategy.

References

1 A. Pevsner et al, Phys. Rev. Lett., **7**: 421 (1961)
2 G. R. Kalbfleisch et al, Phys. Rev. Lett., **12**: 527 (1964)
3 M. Goldberg et al, Phys. Rev. Lett., **12**: 546 (1964)
4 J. Gasser and H. Leutwyler, Annals Phys., **158**: 142 (1984)
5 J. Wess and B. Zumino, Phys. Lett. B, **37**: 95 (1971)
6 E. Witten, Nucl. Phys. B, **223**: 422 (1983)
7 J. Bijnens, A. Bramon, and F. Cornet, Z. Phys. C, **46**: 599 (1990)
8 J. J. Sakurai, Annals Phys., **11**: 1 (1960)
9 L. G. Landsberg, Phys. Rept., **128**: 301 (1985)
10 R. Kaiser and H. Leutwyler, Eur. Phys. J. C, **17**: 623 (2000)
11 M. Ablikim et al (BESIII), Phys. Rev. Lett., **118**: 012001 (2017)
12 M. Ablikim et al (BESIII), Phys. Rev. D, **92**: 012001 (2015)
13 M. Ablikim et al (BESIII), Phys. Rev. D, **92**: 051101 (2015)
14 M. Ablikim et al (BESIII), Phys. Rev. D, **96**: 012005 (2017)
15 M. Ablikim et al (BESIII), Phys. Rev. Lett., **112**: 251801 (2014); Phys. Rev. Lett., **113**: 039903 (2014)
16 M. Ablikim et al (BESIII), Nucl. Instrum. Meth. A, **614**: 345 (2010)
17 C. Patrignani et al (Particle Data Group), Chin. Phys. C, **40**: 100001 (2016)
18 M. Ablikim et al (BESIII), Chin. Phys. C, **36**: 915 (2012)
19 M. Ablikim et al (BESIII), Chin. Phys. C, **41**: 013001 (2017)
20 M. Ablikim et al (BESIII), Phys. Rev. D, **92**: 012014 (2015)
21 D. G. Sutherland, Phys. Lett., **23**: 384 (1966)
22 J. S. Bell and D. G. Sutherland, Nucl. Phys., **B4**: 315 (1968)
23 R. Baur, J. Kambor, and D. Wyler, Nucl. Phys. B, **460**: 127 (1996)
24 C. Ditsche, B. Kubis, and U.-G. Meissner, Eur. Phys. J. C, **60**: 83 (2009)
25 H. Leutwyler, Phys. Lett. B, **378**: 313 (1996)
26 H. Osborn and D. J. Wallace, Nucl. Phys. B, **20**: 23 (1970)
27 J. Gasser and H. Leutwyler, Nucl. Phys. B, **250**: 539 (1985)
28 J. Kambor, C. Wiesendanger, and D. Wyler, Nucl. Phys. B, **465**: 215 (1996)
29 A. V. Anisovich and H. Leutwyler, Phys. Lett. B, **375**: 335 (1996)
30 J. Bijnens and K. Ghorbani, JHEP, **11**: 030 (2007)
31 S. P. Schneider, B. Kubis, and C. Ditsche, JHEP, **02**: 028 (2011)
32 K. Kampf, M. Knecht, J. Novotny, and M. Zdrahal, Phys. Rev. D, **84**: 114015 (2011)
33 G. Colangelo, S. Lanz, H. Leutwyler, and E. Passemar, PoS, **EPS-HEP2011**: 304 (2011)
34 G. Colangelo, S. Lanz, H. Leutwyler, and E. Passemar, Phys. Rev. Lett., **118**: 022001 (2017)
35 P. Guo et al, Phys. Rev. D, **92**: 054016 (2015)
36 F. Ambrosino et al (KLOE), JHEP, **05**: 006 (2008)

37 J. Bijnens and J. Gasser, Phys. Scripta, **T99**: 34 (2002)
38 B. Borasoy and R. Nissler, Eur. Phys. J. A, **26**: 383 (2005)
39 J. G. Layter et al, Phys. Rev. D, **7**: 2565 (1973)
40 A. Abele et al (Crystal Barrel), Phys. Lett. B, **417**: 197 (1998)
41 P. Adlarson et al (WASA-at-COSY), Phys. Rev. C, **90**: 045207 (2014)
42 A. Anastasi et al (KLOE-2), JHEP, **05**: 019 (2016)
43 C. O. Gullstrom, A. Kupsc and A. Rusetsky, Phys. Rev. C, **79**: 028201 (2009)
44 F. Ambrosino et al (KLOE), Phys. Lett. B, **694**: 16 (2011)
45 C. Adolph et al (WASA-at-COSY), Phys. Lett. B, **677**: 24 (2009)
46 S. Prakhov et al (Crystal Ball at MAMI, A2), Phys. Rev. C, **79**: 035204 (2009)
47 M. N. Achasov et al, JETP Lett., **73**: 451 (2001); Pisma Zh. Eksp. Teor. Fiz., **73**: 511 (2001)
48 A. Abele et al (Crystal Barrel), Phys. Lett. B, **417**: 193 (1998)
49 D. Alde et al (Serpukhov-Brussels-Annecy(LAPP), Soviet-CERN), Z. Phys. C, **25**: 225 (1984), [Yad. Fiz., **40**: 1447 (1984)]
50 M. Ablikim et al (BESIII), Phys. Rev. D, **83**: 012003 (2011)
51 M. Ablikim et al (BESIII), arXiv:1709.04627 [hep-ex]
52 R. Escribano, P. Masjuan and J. J. Sanz-Cillero, JHEP, **05**: 094 (2011)
53 V. Dorofeev et al, Phys. Lett. B, **651**: 22 (2007)
54 A. M. Blik et al, Phys. Atom. Nucl., **71**: 2124 (2008), [Yad. Fiz.71,2161(2008)]
55 P. Adlarson et al, arXiv:1709.04230
56 B. Kubis and S. P. Schneider, Eur. Phys. J. C, **62**: 511 (2009)
57 T. Isken, B. Kubis, S. P. Schneider, and P. Stoffer, Eur. Phys. J. C, **77**: 489 (2017)
58 F. G. Binon et al (Serpukhov-Brussels-Annecy(LAPP)), Phys. Lett., **140B**: 264 (1984)
59 D. Alde et al (Serpukhov-Brussels-Los Alamos-Annecy(LAPP)), Z. Phys. C, **36**: 603 (1987)
60 M. Ablikim et al (BESIII), Phys. Rev. Lett., **108**: 182001 (2012)
61 D. J. Gross, S. B. Treiman, and F. Wilczek, Phys. Rev. D, **19**: 2188 (1979)
62 B. Borasoy, U.-G. Meissner, and R. Nissler, Phys. Lett. B, **643**: 41 (2006)
63 P. Naik et al (CLEO), Phys. Rev. Lett., **102**: 061801 (2009)
64 F.-K. Guo, B. Kubis, and A. Wirzba, Phys. Rev. D, **85**: 014014 (2012)
65 D. Parashar, Phys. Rev. D, **19**: 268 (1979)
66 M. Ablikim et al (BESIII), arXiv:1712.01525 [hep-ex]
67 M. Gell-Mann, D. Sharp, and W. G. Wagner, Phys. Rev. Lett., **8**: 261 (1962)
68 W. Bartel et al (JADE), Phys. Lett. B, **113**: 190 (1982)
69 H. J. Behrend et al (CELLO), Phys. Lett. B, **114**: 378 (1982), [Erratum: Phys. Lett.125B,518(1983)]
70 C. Berger et al (PLUTO), Phys. Lett. B, **142**: 125 (1984)
71 M. Althoff et al (TASSO), Phys. Lett. B, **147**: 487 (1984)
72 H. Aihara et al (TPC/Two Gamma), Phys. Rev. D, **35**: 2650 (1987)
73 H. Albrecht et al (ARGUS), Phys. Lett. B, **199**: 457 (1987)
74 S. I. Bityukov et al, Z. Phys. C, **50**: 451 (1991)
75 M. Benayoun et al, Z. Phys. C, **58**: 31 (1993)
76 A. Abele et al (Crystal Barrel), Phys. Lett. B, **402**: 195 (1997)
77 M. Acciarri et al (L3), Phys. Lett. B, **418**: 399 (1998)
78 F. Stollenwerk, C. Hanhart, A. Kupsc, U. G. Meissner, and A. Wirzba, Phys. Lett. B, **707**: 184 (2012)
79 P. Adlarson et al (WASA-at-COSY), Phys. Lett. B, **707**: 243 (2012)
80 D. Babusci et al (KLOE), Phys. Lett. B, **718**: 910 (2013)
81 C. Hanhart, A. Kupsc, U. G. Meißner, F. Stollenwerk, and A. Wirzba, Eur. Phys. J. C, **73**: 2668 (2013); Eur. Phys. J. C, **75**: 242 (2015)
82 G. J. Gounaris and J. J. Sakurai, Phys. Rev. Lett., **21**: 244 (1968)
83 R. Garcia-Martin, R. Kaminski, J. R. Pelaez, J. Ruiz de Elvira, and F. J. Yndurain, Phys. Rev. D, **83**: 074004 (2011)
84 B. Kubis and J. Plenter, Eur. Phys. J. C, **75**: 283 (2015)
85 M. Ablikim et al (BESIII), Phys. Rev. D, **87**: 092011 (2013)
86 A. Faessler, C. Fuchs, and M. I. Krivoruchenko, Phys. Rev. C, **61**: 035206 (2000)
87 B. Borasoy and R. Nissler, Eur. Phys. J. A, **33**: 95 (2007)
88 T. Petri, arXiv:1010.2378 [nucl-th]
89 E. Czerwinski et al, arXiv:1010.2378 [nucl-th]
90 T. Blum et al, arXiv:1311.2198 [hep-ph]
91 V. M. Budnev and V. A. Karnakov, Pisma Zh. Eksp. Teor. Fiz., **29**: 439 (1979)
92 R. I. Dzhelyadin et al, Phys. Lett. B, **88**: 379 (1979); JETP Lett., **30**: 359 (1979)
93 A. Bramon and E. Masso, Phys. Lett. B, **104**: 311 (1981)
94 L. Ametller, L. Bergstrom, A. Bramon, and E. Masso, Nucl. Phys. B, **228**: 301 (1983)
95 L. Ametller, J. Bijnens, A. Bramon, and F. Cornet, Phys. Rev. D, **45**: 986 (1992)
96 H. J. Behrend et al (CELLO), Z. Phys. C, **49**: 401 (1991)
97 C. Terschlüsen, S. Leupold, and M. F. M. Lutz, Eur. Phys. J. A, **48**: 190 (2012)
98 R. Jora, Nucl. Phys. Proc. Suppl., **207-208**: 224 (2010)
99 R. Escribano, PoS, **QNP2012**: 079 (2012)
100 M. Ablikim et al (BESIII), Phys. Rev. D, **87**: 012009 (2013)
101 M. Ablikim et al (BES), Phys. Rev. Lett., **97**: 202002 (2006)
102 M. Ablikim et al (BESIII), Phys. Rev. D, **87**: 032006 (2013)
103 P. Fayet, Phys. Rev. D, **74**: 054034 (2006)
104 P. Fayet, Phys. Rev. D, **75**: 115017 (2007)
105 M. Ablikim et al (BESIII), Phys. Rev. D, **84**: 032006 (2011)
106 C. Jarlskog and E. Shabalin, Phys. Scripta, **T99**: 23 (2002)
107 M. Ablikim et al (BESIII), Phys. Rev. D, **93**: 072008 (2016)
108 L. Bergstrom and H. R. Rubinstein, Phys. Lett. B, **203**: 183 (1988)
109 D. N. Gao, Phys. Rev. D, **96**: 093003 (2017)
110 C. Q. Geng, J. N. Ng, and T. H. Wu, Mod. Phys. Lett. A, **17**: 1489 (2002)
111 D. N. Gao, Mod. Phys. Lett. A, **17**: 1583 (2002)